



## 1 Surface water storage influences streamflow signatures

2  
3 Melanie K. Vanderhoof<sup>1\*</sup>, Peter Nieuwlandt<sup>2</sup>, Heather E. Golden<sup>3</sup>, Charles R. Lane<sup>4</sup>, Jay R.  
4 Christensen<sup>3</sup>, Will Keenan<sup>1</sup>, Wayana Dolan<sup>1</sup>

5  
6 <sup>1</sup>U.S. Geological Survey, Geosciences and Environmental Change Science Center, PO Box 25046, MS 980, Denver  
7 Federal Center, Denver Colorado 80225, USA

8 <sup>2</sup>Delaware Water Gap National Recreation Area, 1978 River Rd, Bushkill, PA 18324, USA

9 <sup>3</sup>Office of Research and Development, U.S. Environmental Protection Agency, 26 W. Martin Luther King Dr.,  
10 Cincinnati, Ohio, 45268, USA

11 <sup>4</sup>Office of Research and Development, U.S. Environmental Protection Agency, 980 College Station Road, Athens,  
12 Georgia 30605, USA

13 *Correspondence to:* Melanie Vanderhoof ([mvanderhoof@usgs.gov](mailto:mvanderhoof@usgs.gov))

14 **Abstract.** Extreme flow conditions in river discharge have far-reaching environmental and economic consequences.  
15 The retention of surface water in lakes, wetlands, and floodplains can potentially moderate these extreme flows by  
16 modifying the timing, duration, and magnitude of flow generation. However, efforts to characterize the impact of  
17 surface water storage on river discharge have been limited in geographic extent. In this analysis, a suite of hydrologic  
18 signatures, quantifying components of watershed flow regimes, was calculated from daily discharge at 72 gaged  
19 watersheds across the conterminous United States. Random forest models were developed to explain variability in six  
20 hydrologic signatures related to flashiness and high and low flow conditions. In addition to traditionally considered  
21 variables such as climate, land cover, topography, and geology, a novel remote sensing (Sentinel-1 & 2) approach was  
22 used to study the contribution of surface water storage dynamics to each signature's variability. While climate variables  
23 explained much of the variability in the hydrologic signatures, models for five of the six signatures showed an  
24 improvement in explanatory power when landscape characteristics were added. Automated variable selection is part  
25 of the modeling process and can be indicative of the relative importance of certain variables over others. When all  
26 variables were considered, four of the six signature models selected remotely sensed inundation variables. The amount  
27 of semi-permanent and permanent floodplain inundation, for example, was both negatively correlated with, and  
28 showed the greatest variable importance for wet season flashiness. Further, increases in seasonal floodplain inundation  
29 were positively correlated with increases in peak flows. This suggests that the storage of surface water on floodplains  
30 is relevant to both flashiness and high flow signatures. In addition, spatial variability in the amount of semi-permanent  
31 and permanent non-floodplain water helped explain variability in the baseflow index. These findings suggest that  
32 watershed surface water storage dynamics explain a portion of streamflow signature variability. The results underscore  
33 the need for protection and restoration of surface water storage systems, such as wetlands, across watersheds.

34  
35 **Keywords:** drought, floodplain, floods, hydrologic signatures, inundation, lakes, non-floodplain wetlands, stream  
36 discharge metrics, wetlands

37



## 38 **Short Summary**

39 Streamflow signatures can help characterize a watershed's response to rainfall and snowmelt events. We explored if  
40 surface water storage-related variables, which are typically excluded from streamflow signature analyses, may help  
41 explain the variability in streamflow signatures. We found that remotely sensed surface water storage watershed  
42 location and hydroperiod were correlated with or explained a portion of the variability in hydrologic signatures across  
43 72 streamflow gages.

## 45 **1 Introduction**

46 The response of streamflow to climate extremes has important environmental and economic implications.  
47 Drought events limit streamflow available for agriculture, drinking water, and wildlife (Stewart et al., 2020; Apurv  
48 and Cai, 2021), and have cost the United States \$53 billion in just the past five years (2019-2023) (NOAA, 2024).  
49 Flood events, meanwhile, can endanger property, infrastructure, and human lives, and have caused global economic  
50 damages exceeding \$1 trillion between 1980 and 2013 (Winsemius et al., 2016). Climate change is altering the  
51 frequency of these hydroclimatic extremes (Heidari et al., 2020) and may also alter how climate extremes propagate  
52 to impact runoff (Wu et al., 2022). In recent years, several studies have shown that surface water storage (e.g.,  
53 wetlands, lakes, ponds), at least in some watersheds, can potentially increase baseflow and decrease peak flows (Rajib  
54 et al., 2020; Wu et al., 2020; Zeng et al., 2020), implying that consideration of surface water storage and storage  
55 dynamics in models could improve predictions of flood and drought impacts (Golden et al., 2021). However, surface  
56 water storage is typically excluded from both hydrological models (Golden et al., 2014; Jones et al., 2019) and analyses  
57 of river and stream hydrologic signatures (Addor et al., 2018; McMillan, 2019). Therefore, our understanding of when  
58 and where surface water storage influences river discharge is still very limited.

59 Hydrologic signatures are quantitative metrics, typically calculated from streamflow time series, that can  
60 describe the magnitude, timing, rate of change, duration, and frequency of flow conditions (Richter et al., 1996; Daigle  
61 et al., 2011; McMillan et al., 2019). Hydrologic signatures are often selected for a specific hydrological or ecological  
62 application or objective. For example, some studies have developed signatures that reflect wet conditions such as  
63 flashiness or seasonal flooding (Hannaford and March, 2008; Hendry et al., 2019), while others have focused on  
64 applying hydrologic signatures to characterize late-season, low flow regimes (Daigle et al., 2011; Kelly and White,  
65 2016), or alternatively, the impact of hydrologic alterations, such as groundwater pumping, flow diversions, or land  
66 use conversion (Richter et al., 1996). The relationship between hydrologic signatures and watershed characteristics,  
67 such as climate and topography, has been characterized using statistical techniques such as correlation analyses  
68 (Berghuijs et al., 2016; Kuentz et al., 2017), random forest models (Trancoso et al., 2016; Addor et al., 2018; Opiel  
69 and Schumann, 2020) and regression functions (van Dijk, 2010; Beck et al., 2015; Kuentz et al., 2017), with studies  
70 finding variability in the model strength between different signatures (Beck et al., 2015; Addor et al., 2018).

71 Previous research has shown that drivers of hydrologic signatures can reflect specific aspects of flow. For  
72 example, signatures that reflect high flow events are often best predicted by climate, including precipitation (van Dijk,  
73 2010; Kuentz et al., 2017), while signatures reflecting baseflow are often linked to geology (Kuentz et al., 2017), as  
74 well as potential evapotranspiration (van Dijk, 2010; Beck et al., 2013). Generally, hydrologic signatures are best



75 explained by climate variables, such as aridity, precipitation, and snowfall (Beck et al., 2015; Addor et al., 2018).  
76 Land cover, such as proportion forest, often acts as a secondary controlling process (Kuentz et al., 2017; Trancoso et  
77 al., 2016; Addor et al., 2018). While Beck et al. (2013) found baseflow to be positively correlated with the average  
78 proportion of open water, and Beck et al. (2015) found slope, which can be indicative of potential water storage  
79 capacity, to be helpful in explaining multiple signatures, efforts to model drivers of hydrologic signatures have rarely  
80 included or considered surface water storage capacity, and have not, to our knowledge, considered surface water extent  
81 dynamics or hydroperiod.

82 Despite surface water storage being infrequently considered in the analysis of hydrologic signatures, it is  
83 widely accepted that wetlands and lakes have a significant influence on the hydrologic cycle (Bullock and Acreman,  
84 2003). In watersheds lacking surface water storage (e.g., lakes, ponds, reservoirs, and wetlands) when precipitation  
85 falls, it is captured by vegetation, infiltrates the soils, or is transported downgradient as infiltration-excess or  
86 saturation-excess runoff (Eamus et al., 2006). Conversely, in watersheds where surface storage availability exists,  
87 precipitation, snow water equivalent and runoff can be stored and gradually released through time from both floodplain  
88 and non-floodplain storage - via groundwater baseflow, fill-spill surface runoff, or merging with streams via fill-and-  
89 spill mechanisms (Rains et al., 2016; Fritz et al., 2018; Lane et al., 2018; Stepchinski et al., 2023), creating a less  
90 “flashy” system (Shaw et al., 2012; Kuppel et al., 2015). Surface storage areas, both within and outside of the  
91 floodplain, can also contribute to streamflow when stream-connected water bodies rise, subsuming nearby, previously  
92 disconnected storage systems, e.g., upland wetlands (Vanderhoof et al., 2016). The influence of these disconnected  
93 systems, e.g., upland wetlands, can depend on the position of the wetlands relative to the stream network as well as  
94 watershed characteristics (Fritz et al., 2018; Lane et al., 2018; Wu et al., 2020). Although we know that lakes and  
95 wetlands can withhold and contribute water to river networks, it is less clear if surface water storage across multiple  
96 watersheds and regions has a measurable impact on river discharge dynamics.

97 Our limited understanding of how surface water storage dynamics impact river discharge is in part  
98 attributable to surface water storage being traditionally ignored by hydrologic models (Golden et al., 2014; Jones et  
99 al., 2019). In recent years, studies have shown that integrating wetlands, particularly non-floodplain wetlands, into  
100 hydrologic models can improve streamflow simulation accuracy (Rajib et al., 2020; Golden et al., 2021). While recent  
101 modeling studies have been limited in spatial extents, have simplified wetland volume estimates, and have relied, most  
102 commonly, on topographic estimates of potential water storage, each have demonstrated that surface water storage  
103 can potentially increase baseflow (McLaughlin et al., 2014; Zeng et al., 2020) as well as potentially reduce peak flow  
104 and flood duration (Evenson et al., 2018; Ameli and Creed, 2019; Wu et al., 2020).

105 Further research is needed to improve our understanding of when and where dynamic surface water storage  
106 influences river discharge across multiple diverse watersheds and regions. Here, we calculated a suite of hydrologic  
107 signatures to characterize variability in flow flashiness and high and low flow conditions across 72 diverse watersheds  
108 in the contiguous United States (CONUS). We developed two random forest models for each flow signature: one  
109 representing climate variables only and one representing climate, land cover, geology, topographic, and surface water  
110 storage input variables. This approach helped us to assess the relative ability of climate alone, compared to catchment  
111 characteristics that uniquely included novel remotely sensed surface water extent and hydroperiod, to explain the



112 variability in hydrologic signatures. Specifically, our research questions were: (1) What are the dominant explanatory  
113 variables explaining the variability in flow flashiness and high and low flow condition-related hydrologic signatures  
114 across watersheds representing different climates, topography, and land covers? and (2) To what extent do surface  
115 water storage-related variables correlate with or help explain variability in these selected hydrologic signatures?

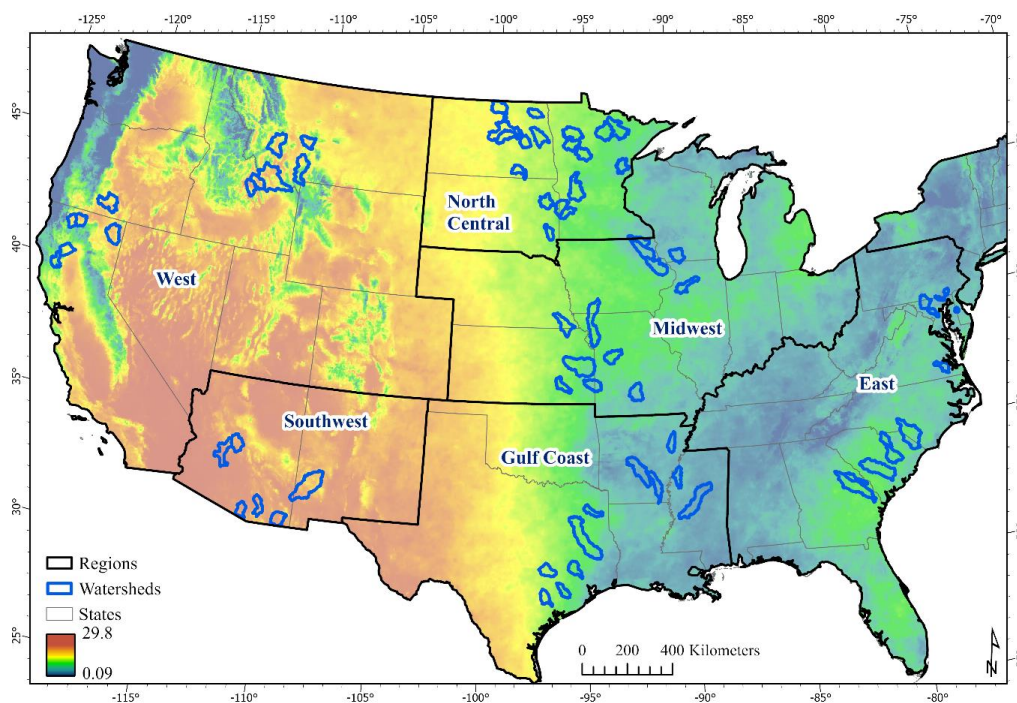
## 116 **2. Materials and Methods**

### 117 **2.1 Watersheds**

118 A total of 72 U.S. Geological Survey (USGS) stream gages and associated watersheds (Fig. 1) were selected  
119 across the conterminous U.S. (CONUS) from the GAGES-II dataset (Falcone 2011). Gaged watersheds, to the extent  
120 possible, were selected to be approximately co-located with regions used to train the Sentinel-1 and Sentinel-2  
121 satellite-based surface water algorithms to maximize the accuracy of the algorithms (Vanderhoof et al., 2023). The  
122 algorithms were used to map surface water extent over time at each of the watersheds. Watersheds with tidal wetlands  
123 were excluded to focus on freshwater aquatic systems. Further, potential watersheds were reviewed to minimize the  
124 inclusion of major dams, defined as dams 15.2 meters or more in height (storage capacity of 6.17 million cubic meters)  
125 near watershed outlets (National Atlas of the United States, 2006). While most watersheds, 80%, were between 1500  
126 km<sup>2</sup> and 5000 km<sup>2</sup>, watersheds ranged in size from 292 km<sup>2</sup> to 9918 km<sup>2</sup>.

127 Across the selected watersheds, stream density, as calculated from the National Hydrography Dataset (NHDplus)  
128 high resolution dataset (USGS, 2022), ranged from 259 m km<sup>-2</sup> to 4182 m km<sup>-2</sup> across the selected watersheds, with a  
129 median density of 1461 m km<sup>-2</sup> (Table A1). The proportion of each watershed classified as wetland by the National  
130 Wetland Inventory (NWI) dataset (USFWS, 2019) ranged from 1.1% to 48.7% with a median wetland proportion of  
131 5.6% (Table A1). Mean annual precipitation (2016-2023) ranged from 325 mm to 1659 mm, with a median annual  
132 average of 967 mm (GRIDMET; Abatzoglou, 2013). In addition, the dominant landcover class was cultivated crops  
133 or hay/pasture for 36 of the watersheds, with other dominant classes including forest (18 watersheds) and grassland-  
134 shrub/scrub (13 watersheds) (Homer et al., 2020; Table A1). The watersheds were grouped by U.S. region, including  
135 West, Southwest, North Central, Gulf Coast, Midwest, and East, to facilitate data interpretation (Fig. 1).

136



137  
138  
139  
140  
141

**Figure 1.** Selected U.S. Geological Survey (USGS) gaged watersheds in relation to aridity (2016-2023), defined as annual actual evapotranspiration divided by annual precipitation, where maroon/orange indicates arid conditions and blue indicates less arid conditions.

## 142 2.2 Hydrologic signatures: response variables

143 Hydrologic signatures were calculated from daily discharge at each gage and were used as the response  
144 variables in our statistical analyses (Table 1). Daily rate of stream discharge was acquired from the USGS National  
145 Water Information System for 2016-2023 (USGS, 2024). The period was limited by the temporal availability of  
146 Sentinel-2 imagery (Sentinel-2a and -2b launched in June 2015 and March 2017, respectively), required for the  
147 surface water algorithm. Signatures were selected from the literature to represent discharge extremes (high flow and  
148 low flow) as well as variability in discharge. Signatures related to characterizing high flow conditions included a (1)  
149 wet season flashiness index, where flashiness reflected daily variability in discharge within the wet season, defined  
150 as the three months in each year with the highest average discharge (Baker et al., 2004). (2) The maximum annual  
151 30-day flow per drainage area (km<sup>2</sup>) (MAX30/area) reflected seasonal peaks in discharge (Hannaford and Marsh,  
152 2008); and (3) discharge exceeded 10% of the time, within a given year (Q10) minus discharge exceeded 95% of the  
153 time (Q95), within a given year ((Q10-Q95)/area) and averaged over multiple years, or the difference between high  
154 flows and the baseflow regime (National River Flow Archive, 2024). The (4) flashiness index, which reflected daily  
155 variability in discharge across seasons, was included as a metric on how rapidly a watershed responds to  
156 precipitation or snowmelt events (Baker et al., 2004). Low flow conditions were characterized using (5) a baseflow  
157 index (USFS, 2022), calculated as the ratio of the average annual baseflow volumes to the average annual flow



158 volumes, and (6) the average driest month discharge per area (DryMonth/area, Daigle et al., 2011) (Table 1).  
159 Signatures were either calculated to be unitless or divided by the drainage area (km<sup>2</sup>) so that they could be compared  
160 across watersheds (Daigle et al., 2011). The distribution of hydrologic signature values was evaluated using the  
161 Shapiro-Wilk test for normality. Variables with extreme outliers were normalized using log<sub>10</sub> transform (Beck et  
162 al., 2015) and included the flashiness index and wet season flashiness index. To evaluate how the hydrologic  
163 signatures may depend on the analysis period selected, the signatures from the 8-year period (2016-2023), that  
164 corresponds with the time period of available imagery, were contrasted with signatures derived from daily discharge  
165 over a 24-year period (2000-2023), using Pearson correlation and relative bias.

## 166 **2.3 Independent variables**

### 167 **2.3.1 Climate variables**

168 Climate variables were averaged over the 2016-2023 period. Total annual, average precipitation and actual  
169 evapotranspiration (ET) were derived from the daily University of Idaho Gridded Surface Meteorological Dataset  
170 (GRIDMET, 4 km resolution; Abatzoglou, 2013; Table 2). An aridity index was calculated as annual total ET divided  
171 by annual total precipitation, where higher values represent arid watersheds and lower values represent less arid  
172 watersheds (Budyko, 1958), and water availability was evaluated as annual precipitation – annual ET. Maximum daily  
173 temperature was derived from DAYMET, which has been found to outperform GRIDMET for temperature  
174 (Mehdipoor et al., 2018), and variables included temperature seasonality, defined as the difference between average  
175 summer (June, July, August) maximum temperature and average winter (December, January, February) maximum  
176 temperature, as well as the maximum temperature coefficient of variation (CV). A precipitation CV and precipitation  
177 seasonality were also included, using DAYMET daily precipitation, since DAYMET includes daily estimates of snow-  
178 water equivalent (Table 2). DAYMET variables relied on 2016-2022 data, as 2023 was not yet available at the time  
179 of the analysis. To contextualize the climate conditions reflected in the 8-year period, (1) the GRIDMET 5-day Palmer  
180 Drought Severity Index values (PDSI; Abatzoglou, 2013) for the 2016-2023 period at each watershed were compared,  
181 using rank percentile, to the past 44 years (1980-2023).



182 **Table 1.** Hydrological signatures included in the analysis. MAX: maximum

Signature	Targeted flow regime	Calculation	Units	Median	Min	Max	Source
Flashiness index	All flows	The sum of the absolute value of the changes in discharge from the day prior to the current day (discharge $t_2$ – discharge $t_1$ ) divided by the sum of the daily discharge values (log normalized).	Unitless	-0.81	-1.63	0.23	(Baker et al., 2004)
Flashiness index (wet season)	High flows	The sum of the absolute value of the changes in discharge from the day prior in the three wettest months (highest discharge) divided by the sum of daily discharge values in those months (log normalized).	Unitless	-0.84	-1.89	0.23	(Baker et al., 2004)
MAX30/area	High flows	The flow rate for the 30 days per year with the highest flow rate, summed over the 30 days, and averaged per year, divided by the watershed area.	m <sup>3</sup> /sec/km <sup>2</sup>	0.94	0.01	3.48	(Hannaford and Marsh, 2008)
(Q10-Q95)/area	High flows	Discharge exceeded 10% of the time (Q10) minus discharge exceeded 95% of the time (Q95), divided by watershed area.	m <sup>3</sup> /sec/km <sup>2</sup>	0.016	0.000	0.056	(National River Flow Archive, 2024)
DryMonth/area	Low flows	Average annual discharge in the driest month (excluding snow cover months) divided by watershed area.	m <sup>3</sup> /sec/km <sup>2</sup>	0.0019	0.0000	0.0112	(Daigle et al., 2011)
Baseflow index	Low flows	The ratio of the average daily flow during the lowest annual 7-day flow (excluding snow cover conditions) to the annual average daily flow.	Unitless	0.19	0.00	0.70	(USFS, 2022)

183 **2.3.2 Land cover, soils, topography, and wetland variables**

184 Vegetation was represented by the 2019 National Land Cover Database (NLCD), as the proportion of each  
 185 watershed classified as (1) forest (evergreen, deciduous, or mixed), (2) developed, and (3) cultivated crops (Homer et  
 186 al., 2020). Annual minimum depth to water table, average soil thickness, fraction clay and fraction sand were derived  
 187 from the Soil Survey Geographic Database (SSURGO; Falcone, 2011). To represent topography, the percent slope  
 188 and elevation range divided by average elevation were derived using the 10 m USGS Digital Elevation Model (DEM)  
 189 (Table 2). The average watershed topographic diversity was also considered, calculated from the multi-scale  
 190 Topographic Position Index (mTPI) and the Continuous Heat-Insolation Load Index (CHILI, 30 m; Theobald et al.,  
 191 2015). Stream density was calculated using the total stream length, defined by the NHDplus high resolution dataset  
 192 (USGS, 2022). The National Wetland Inventory dataset (USFWS, 2019) was used to calculate the proportion of each  
 193 watershed mapped as wetlands. The floodplain variable was defined as the proportion of each watershed classified as  
 194 within the 100-year floodplain (Woznicki et al., 2019). Lastly, the connectivity of wetlands to streams can influence  
 195 the timing of water moving into the stream network, so the proportion of each watershed mapped as geographically  
 196 isolated wetlands (GIWs; Leibowitz, 2015), or non-floodplain wetlands (NFW), that are surrounded by upland, as  
 197 well as the proportion of total wetland area mapped as GIWs was considered (Lane and D’Amico, 2016).

198 **2.3.3 Inundation variables**

199 In addition to including non-temporal water variables, such as wetland area, remote sensing platforms allow us  
 200 to include variables that characterize the hydroperiod of surface water stored within watersheds, including lakes,  
 201 ponds, wetlands, and temporary inundation in flood prone areas. Although Landsat can provide a longer temporal  
 202 record of surface water dynamics, observations are limited to periods free of clouds, snow, and ice, which can limit  
 203 the accuracy of temporary and seasonal patterns of inundation. Alternatively, the more frequent Sentinel-2 revisit, and



204 incorporation of a SAR satellite, like Sentinel-1, can help bypass these limitations. Sentinel-1 and Sentinel-2 based  
205 algorithms that map non-water, open water and vegetated water were previously developed using gradient boosted  
206 classifier algorithms for 12 sites across the conterminous U.S. (20 m resolution; Vanderhoof et al., 2023). Details on  
207 the surface water algorithms can be found in Vanderhoof et al., (2023). In this effort individual Sentinel-1 and Sentinel-  
208 2 images, collected between January 1, 2016, and December 31, 2023, overlapping each of the gaged watersheds  
209 ( $n=72$ ) were classified into open water, vegetated water, and non-water. The classified Sentinel-1 and classified  
210 Sentinel-2 time series were consolidated at a 14-day time step where pixel values were assigned as the majority  
211 classification, water (defined as open water plus vegetated water), or non-water (Fig. 2). If, observations of water and  
212 non-water were equal, then open water was prioritized followed by non-water, and lastly vegetated water (Fig. 2),  
213 consistent with the higher accuracy of the open water class relative to the vegetated water class (Vanderhoof et al.,  
214 2023). Where no valid observations were present in the 14-day period, pixels were gap-filled using observations from  
215 the  $t-1$  and  $t+1$  timestep, as shown in Fig. 2.

216 To limit commission error in the surface water time series, a water mask, defined as the maximum allowable  
217 surface water extent, was derived for each watershed, and applied across the time series. Pixels classified as water  
218 outside of the water mask were re-classified as non-water. To generate each water mask, the Sentinel-1 open water  
219 and vegetated water, and Sentinel-2 open water, and vegetated water percentile rasters were manually reviewed for  
220 each watershed (Fig. 2). Percentile thresholds were selected, below which the frequency of erroneously classified  
221 water pixels visually exceeded the frequency of correctly classified water pixels (Table A2). To help inform the  
222 threshold selection, ancillary data were used including the NWI dataset (USFWS, 2019), the 2019 NLCD (Homer et  
223 al., 2020), and base map imagery, delivered through ArcMap. The spatial extent where water pixels were retained was  
224 defined as pixels located within the 100-year floodplain (Woznicki et al., 2019), to account for short-term flood events,  
225 or pixels where the water percentile was greater than the selected threshold in any of the four 5-year percentile rasters  
226 (Table A2). The Sentinel-1 algorithm has a documented omission and commission error of 3.1% and 0.9% for open  
227 water, and a 28.4% and 16.0% commission error for vegetated water, respectively, while the Sentinel-2 algorithm has  
228 an omission and commission error of 3.1% and 0.5% for open water, and a 10.7% and 7.9% commission error for  
229 vegetated water, respectively, when validated against 36 high-resolution images (i.e., WorldView-2, WorldView-3,  
230 PlanetScope) (Vanderhoof et al., 2023). When consolidated at a monthly time-step to a S1-S2 water, non-water  
231 classification, errors of omission and commission for monthly surface water extent averaged 1.6% and 10.4%,  
232 respectively, when validated against 64 PlanetScope images (Vanderhoof et al., 2024). The use of a water mask was  
233 previously shown to reduce commission error, resulting in errors of omission and commission of 1.9% and 6.5%,  
234 respectively for the monthly surface water extent (Vanderhoof et al., 2024).

235 After gap-filling and applying the water masks, the time series for each watershed was then consolidated into an  
236 8-year percentile. Categories of surface water, using the percent of watershed area, were defined in reference to the  
237 100-year floodplain (Woznicki et al., 2019), and included, (1) temporarily flooded, defined as an average of  $\geq 3$  days  
238 but  $< 1$  month per year (Cowardin et al., 1979; Scott et al., 2019), (2) seasonally flooded, defined as inundated  $> 1$   
239 month but  $< 6$  months per year, on average, and (3) semi-permanently and permanently inundated, defined as  $> 6$   
240 months per year, on average (Cowardin et al., 1979; Donnelly et al., 2019) (Table 2). The total amount of inundation





241 of any hydroperiod within the 100-year floodplain, and outside of the 100-year floodplain was also included (Table  
 242 2). The terms surface water extent and inundation are used interchangeably in this analysis.

243

244 **Table 2.** Independent variables considered modeling hydrological signatures. DEM: Digital elevation model, SRTM:  
 245 Shuttle Radar Topography Mission, NLCD: National Land Cover Database, SSURGO: Soil Survey Geographic  
 246 Database, NHD: National Hydrography Dataset

Variable Type	Variable	Units	Min	Max	Median	Source
Climate	Precipitation (P, annual)	mm	325.3	1659.1	967.4	GRIDMET (Abatzoglou, 2013)
	Evapotranspiration (ET, annual)	mm	714	1934.1	1181.1	GRIDMET (Abatzoglou, 2013)
	Aridity index (ET/P, annual)	unitless	0.84	5.88	1.27	GRIDMET (Abatzoglou, 2013)
	Water demand (P - ET, annual)	mm	-1586	265.6	-247.4	GRIDMET (Abatzoglou, 2013)
	Precipitation seasonality	mm	-396	276.6	105	DAYMET (Thornton et al., 2020)
	Precipitation coefficient of variation	mm	196.5	371.8	260.4	DAYMET (Thornton et al., 2020)
	Temperature seasonality	°C	15.6	34.2	23	DAYMET (Thornton et al., 2020)
	Temperature coefficient of variation	°C	26	151	57	DAYMET (Thornton et al., 2020)
Land cover	Forest (evergreen, deciduous, mixed)	% of area	0.059	56.1	17.5	NLCD (2019; Homer et al., 2020)
	Developed (low, medium, high intensity, open space)	% of area	0.323	35.7	4.69	NLCD (2019; Homer et al., 2020)
	Cultivated crops	% of area	0.0	84.7	17.9	NLCD (2019; Homer et al., 2020)
	Stream density	m km <sup>2</sup>	259.2	4181.6	1460.9	NHDPlus High Resolution (USGS, 2022)
Sub-surface	Clay fraction	fraction	0.08	0.47	0.23	SSURGO (Falcone 2011)
	Sand fraction	fraction	0.07	0.74	0.33	SSURGO (Falcone 2011)
	Average soil thickness	cm	81.3	152.4	145.8	SSURGO (Falcone 2011)
	Annual minimum depth to water table	meters	0.49	1.83	1.40	SSURGO (Falcone 2011)
Topography	Slope	%	0.5	32.5	3.7	DEM (Gesch et al., 2002)
	$(\text{Elevation}_{\text{max}} - \text{Elevation}_{\text{min}}) / \text{Elevation}_{\text{average}}$	unitless	0.2	4.9	1.0	DEM (Gesch et al., 2002)
	Global SRTM topographic diversity	unitless	0.03	0.7	0.1	(Theobald et al., 2015)
Inundation Dynamics	Temporarily flooded, floodplain (3 days - 1 month)	% of area	0.07	4.16	0.65	(Vanderhoof et al., 2023)
	Temporarily inundated, non-floodplain (3 days - 1 month)	% of area	0.03	5.85	1.29	(Vanderhoof et al., 2023)
	Seasonally inundated, floodplain (1 - 6 month)	% of area	0.04	8.58	1.77	(Vanderhoof et al., 2023)
	Seasonally inundated, non-floodplain (1 - 6 month)	% of area	0.01	45.81	4.07	(Vanderhoof et al., 2023)
	Semi-permanently and permanently inundated, floodplain (>6 month)	% of area	0	3.54	0.39	(Vanderhoof et al., 2023)
	Semi-permanently and permanently inundated, non-floodplain (>6 month)	% of area	0	5.55	0.44	(Vanderhoof et al., 2023)
	Total floodplain inundation	% of area	0.42	15.46	3.08	(Vanderhoof et al., 2023)
	Total non-floodplain inundation	% of area	0.04	52.59	6.06	(Vanderhoof et al., 2023)
Wetland	Geographically Isolated Wetlands (GIW)	% of area	0.0	9.4	0.6	(Lane and D'Amico 2016)
	Proportion of wetland area identified as GIW	% of area	0.6	80.9	11.4	(Lane and D'Amico 2016; USFWS 2019)
	Floodplain	% of area	1.2	36.8	7.7	(Woznicki, et al., 2019)
	National Wetland Inventory (NWI) wetlands	% of area	1.1	48.7	5.6	NWI (USFWS 2019)

247



## 248 2.4 Modeling analysis

249 The relationships between multiple predictor variables and hydrologic signatures were modeled with random  
250 forest regressions developing using the ‘sklearn’ python package (Pedregosa et al., 2011). For each hydrologic  
251 signature, random forest models were generated that (1) considered the inclusion of climate-related variables only  
252 ( $M_{\text{Climate}}$ ), and (2) considered inclusion of all variables, including climate, topographic, land cover, and wetland and  
253 inundation related variables ( $M_{\text{All}}$ ) (Table 2). The multi-model approach furthered our ability to quantify the relative  
254 contribution of different variable types to explain variability in the hydrologic signatures.

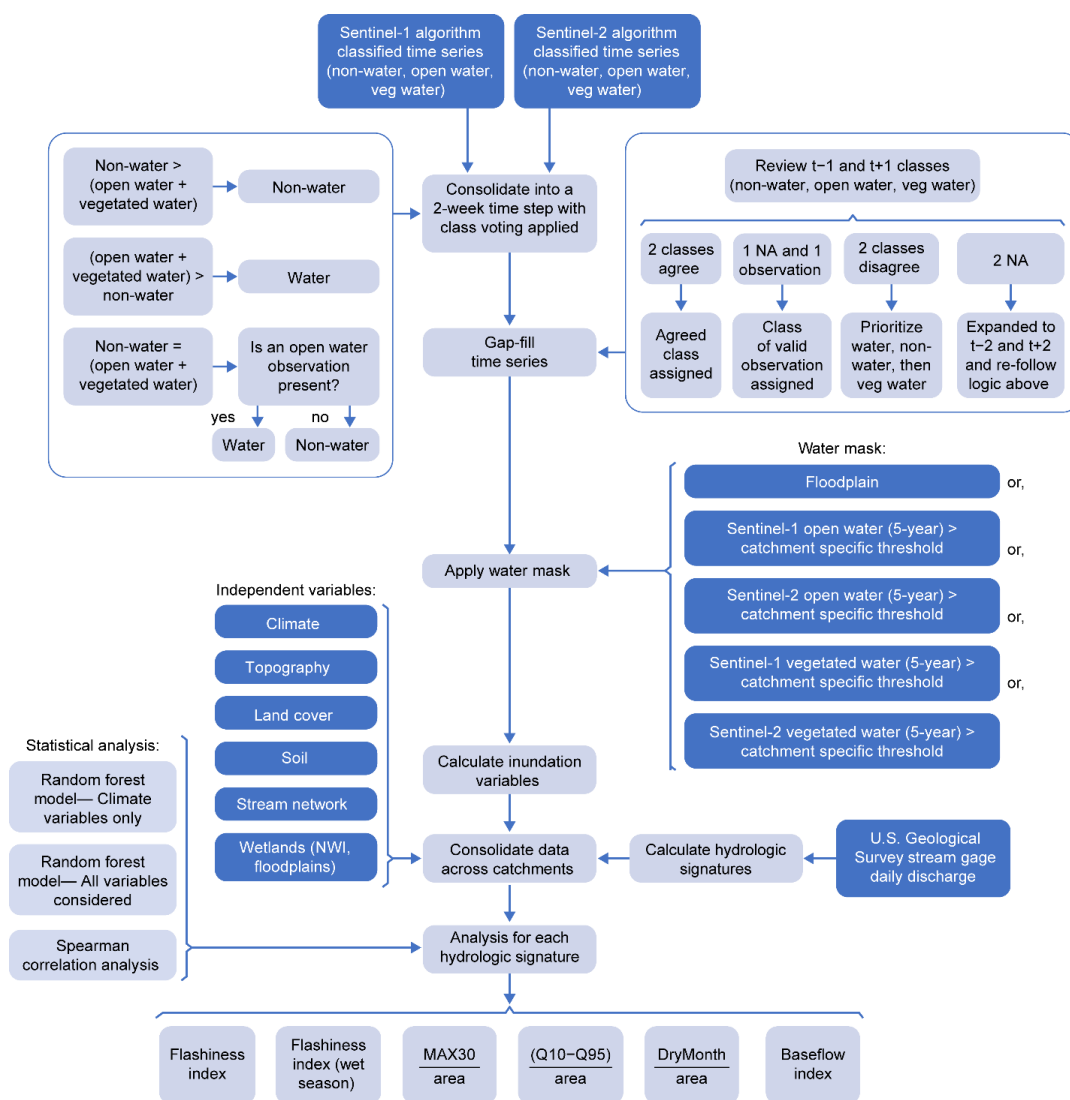
255 Random forest models use a bootstrapping approach to generate hundreds of regression trees and make no prior  
256 assumptions about cause-and-effect relationships or correlations among variables (Hastie et al., 2009). They have also  
257 been previously used in the analysis of hydrologic signatures (e.g., Trancoso et al., 2016; Addor et al., 2018; Opper  
258 and Schumann, 2020). While random forest techniques are generally insensitive to multicollinearity, the inclusion of  
259 highly correlated variables can make it more challenging to identify the most predictive variables, deflate or bias  
260 variable importance values, and complicate model interpretation (Murphy et al., 2010; Gregorutti et al., 2016).  
261 Conversely, an automated variable selection can be indicative of the relative importance of certain variables over  
262 others (Murphy et al., 2010). A stepwise forward selection routine was implemented where the set of potential  
263 predictors were sequentially tested. The predictor that contributed most to reducing the RMSE was selected. During  
264 each step, the remaining predictors were removed if they had a correlation value of 0.8 or greater with any of the  
265 selected predictors. This process was iterated until the improvement in the model’s RMSE was  $<0.001$  with any  
266 additional variables (Sherrouse and Hawbaker, 2023).

267 For each model the variable and hyperparameter selection process were concurrently run, where the potential  
268 models were compared using a nested cross-validation, KFold with 6 splits (Cawley and Talbot, 2010). The  
269 hyperparameters tested were  $n_{\text{estimators}}$  (the number of trees in the forest with tested values of 300, 500, 700, and  
270 1000),  $\text{max\_depth}$  (the maximum depth of a tree with tested values of 2, 3, and 4). For all models,  $\text{max\_features}$  (the  
271 number of features to consider when looking for the best split) was set at the square root of the number of features,  
272 and  $\text{max\_samples}$  (the proportion of samples selected to train each estimator) was set at 0.8. The model with the  
273 highest cross-validated adjusted  $R^2$  was selected.

274 Random forest models do not consider the spatial pattern between samples, therefore any clustering of the  
275 watersheds included in the analysis could potentially bias model predictions (Hengl et al., 2018). The residuals of each  
276 selected model were tested for spatial autocorrelation using Moran’s I (Klute et al., 2002). Of the random forest model  
277 residuals, 5 out of 12 showed significant ( $p < 0.01$ ) spatial autocorrelation, therefore an autocovariate, or additional  
278 model term, representing the mean neighborhood (defined as within 500 km of the catchment center, reflecting  
279 catchment clusters) model residual value, was included in the subset of models to account for spatial dependency  
280 (Betts et al., 2006). Performance of final random forest models was evaluated using the leave-one-out cross validation  
281 to account for the limited sample size ( $n=72$ ) (Vabalas et al., 2019), and the cross-validated model RMSE,  $R^2$ , adjusted  
282  $R^2$ , to account for differences in the number of variables selected. Variable importance was calculated with Python  
283 Scikit-learn as the permutation importance. Single variable correlations between the hydrologic signatures and the



284 predictor variables were also calculated using the non-parametric Spearman Rank Correlation Coefficient, as  
 285 previously used by Berghuijs et al. (2016). Because of the number of comparisons, a Bonferroni correction was applied  
 286 before significance was determined (Emerson, 2020).  
 287



288  
 289

**Figure 2.** Flowchart of steps to generate the surface water variables and data analysis.



290 **3. Results**

291 **3.1 Climate and flow signature temporal context**

292 The minimum (i.e., driest), maximum (i.e., wettest) and median per watershed PDSI rank percentiles for  
293 2016-2023, relative to 1980-2023, averaged 5%, 100%, and 62%, respectively, where 50% represents the median  
294 PDSI for the 1980-2023 period (Table A1). This indicated that the period was slightly wetter, on average, relative to  
295 the longer 44-year period, and that most watersheds exhibited a large range of PDSI conditions (maximum –  
296 minimum) over the 2016-2023 period.

297 While the period used was limited by the available Sentinel-1 and Sentinel-2 image record, signature  
298 uncertainty can increase when using shorter flow records (Kennard et al., 2010). Between-site variability in the  
299 hydrologic signatures derived from the 8-year period, was highly correlated with the between-site variability from a  
300 longer, 24- year period (2000-2023) (Table 3). The median value of hydrologic signatures showed some differences  
301 between the 8-year period (2016-2023) and the longer 24-year period (2000-2023). While both flashiness indices had  
302 a bias of <1%, the MAX30/area and (Q10-Q95)/area had a relative bias of 13.5% and 8.7%, respectively, indicating  
303 that average peak wetness conditions were wetter within the 8-year period, relative to the longer period. Additionally,  
304 the baseflow index and DryMonth/area showed a relative bias of -11.8% and -2.2%, indicating that these signatures  
305 reflected drier conditions, on average, within the 8-year period, relative to the longer period (Table 3). While the  
306 hydrologic signatures of the high and low flow conditions were amplified during the selected period, the signature  
307 values between the two periods were highly correlated, with Pearson *R* correlation values ranging from 0.94 to 0.99  
308 (Table 3). This suggests that the relative variations in hydrologic signature values between the long-term flow records  
309 (24 years) compared to the study period (8 years) are tightly associated. We considered this a solid justification for  
310 using the 8-year Sentinel data availability period for our analyses.

311

312 **Table 3.** Pearson correlation values comparing the 2016-2023 hydrologic signatures with the same signatures derived  
313 from the 2000-2023 period. The relative bias compares the paired signature values from each watershed. All *R* values  
314 were significant at  $p < 0.01$ . MAX: maximum

Metric	R (2016-2023 vs 2000-2023)	Median relative bias (%)
Flashiness index	0.99	0.9
Flashiness index (wet season)	0.99	0.2
MAX30/area	0.97	13.5
(Q10-Q95)/area	0.98	8.7
DryMonth/area	0.94	-2.2
Baseflow index	0.95	-11.8

315



### 316 3.2 Flashiness signatures

317 The flashiness and wet season flashiness signatures reflect how quickly discharge changes in response to  
318 episodic rainfall and snowmelt events, over the course of the year and within the wet season, respectively. Despite  
319 representing different portions of the year, the two signatures were highly correlated ( $R = 0.97$ ,  $p < 0.01$ ). Flashiness  
320 and wet season flashiness were highest, on average, in the Southwest watersheds, and lowest in the West and North  
321 Central watersheds (Table A3, Fig. 3). Watershed flashiness and wet season flashiness were significantly correlated  
322 with very few of the independent variables considered. Most prominently, both significantly ( $p < 0.01$ ) decreased with  
323 an increase in areas mapped as semi-permanently and permanently inundated within the floodplain, and with increases  
324 in total area classified as wetland by the NWI dataset (Table 4). Correlations with climate variables were weaker  
325 relative to the other hydrologic signatures explored. The flashiness index and wet season flashiness index  $M_{All}$  models  
326 improved by 4.28% and 9.97%, respectively, in explanatory power and associated decreases in the RMSE, relative to  
327  $M_{Climate}$ , or when landscape and water variables were added for consideration (Table 5). Variability in the flashiness  
328 signature was best explained by the temperature CV, annual minimum depth to the water table, slope, and amount of  
329 semi-permanent-permanent inundation within the floodplain. The wet season flashiness  $M_{All}$  model selected similar  
330 variables, but the amount of semi-permanent-permanent floodplain inundation had the greatest variable importance  
331 (Table 6; Fig. 4a). Improvement in model predictions, both across the year as well as in the wet season (Fig. 5a), were  
332 explained in part by more semi-permanently to permanently inundated water in the floodplain.

### 333 3.3 Peak flow signatures

334 Peak flow signature values,  $MAX30/area$  and  $(Q10-Q95)/area$ , were highest, on average, within the Gulf  
335 Coast watersheds, and lower, on average, within the Southwest, North Central, and West watersheds, although both  
336 signatures saw a higher degree of variability across the West region (Table A3, Fig. 3). The two signatures were  
337 positively correlated ( $R = 0.93$ ,  $p < 0.01$ ). In relation to the independent variables considered, both signatures,  
338  $MAX30/area$  and  $(Q10-Q95)/area$ , were most highly positively correlated with precipitation and water demand (P-  
339 ET), and negatively correlated with aridity (ET/P) (Table 4). The  $MAX30/area$  and  $(Q10-Q95)/area$  were also  
340 significantly correlated with 4 and 3 remotely sensed inundation variables, respectively. An example of the Spearman  
341 rank correlation of  $(Q10-Q95)/area$  in relation to seasonally inundated area in the floodplain ( $R = 0.69$ ,  $p < 0.01$ ) is shown  
342 in Fig. 4b. The high flow signatures had a positive, significant ( $p < 0.01$ ) correlation with the total amount of inundation  
343 within the floodplain, the amount of seasonal inundation in the floodplain, and the amount of temporary inundation  
344 outside of the floodplain (Table 4). These correlation values were equivalent to or exceeded correlation with existing  
345 water variables, specifically the 100-year floodplain (Table 4). The  $M_{Climate}$  and  $M_{All}$  models for both signatures were  
346 best explained by annual precipitation, followed by the aridity index (ET/P) or water demand (P-ET) (Table 6). Despite  
347 the high explanatory power of climate variables for both high flow signatures, the  $M_{All}$  models improved by 2.73%  
348 and 6.31%, relative to the  $M_{Climate}$  models, for  $MAX30/area$  and  $(Q10-Q95)/area$ , respectively. The  $(Q10-Q95)/area$   
349  $M_{All}$  model added only stream density, while the landscape-based variables for  $MAX30/area$  included forest, stream  
350 density, clay fraction, and the amount of temporarily flooded area within the floodplain (Table 6). Greater area



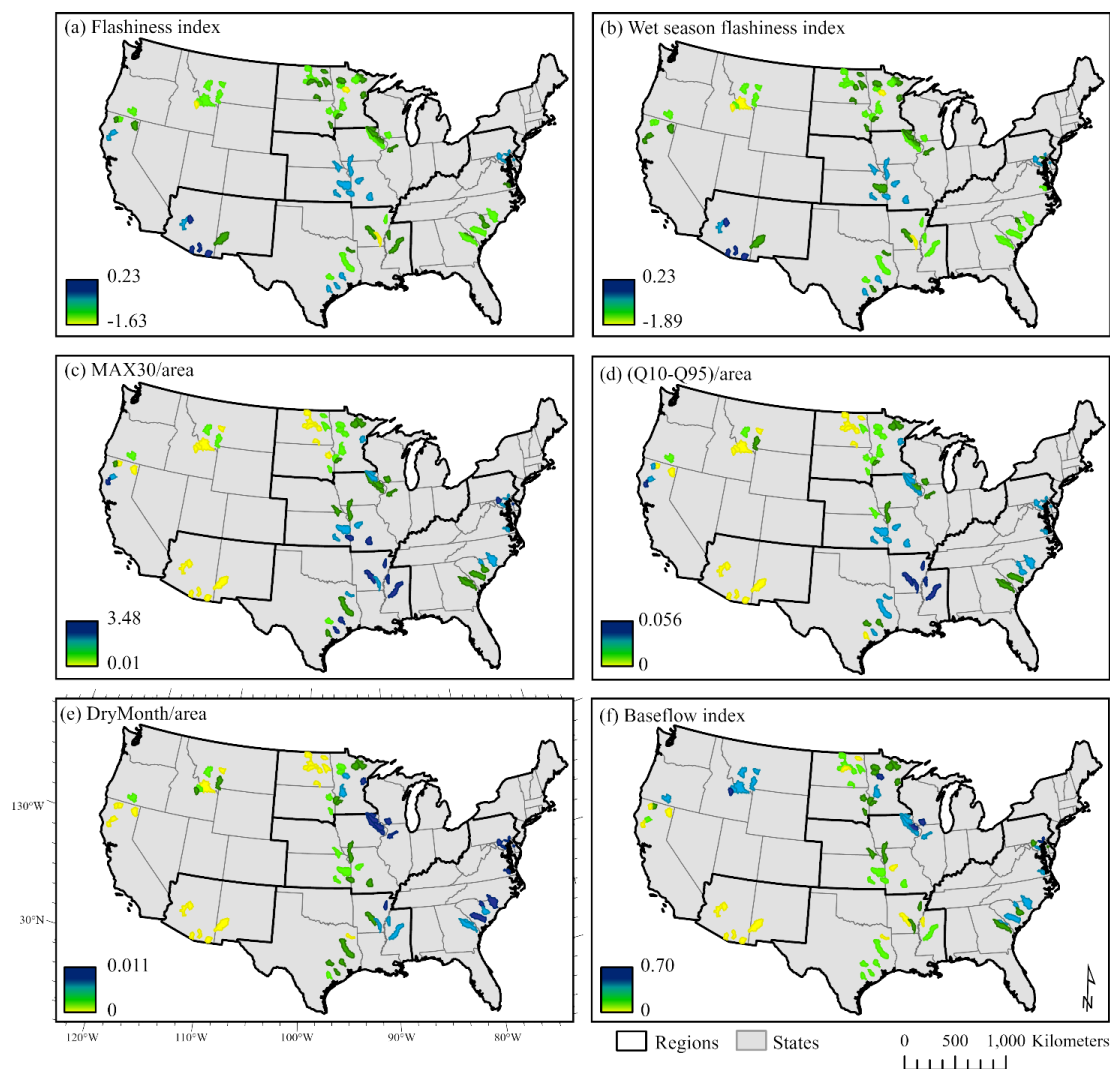
351 temporarily flooded within the floodplain was also significantly positively correlated ( $p < 0.01$ ) with the MAX30/area  
352 (Table 4).

### 353 3.4 Low flow signatures

354 The DryMonth/area and baseflow index were highest within the East watersheds, on average, and lowest  
355 within the Southwest watersheds (Table A3, Fig. 3). Watersheds were also regionally variable. For example,  
356 DryMonth/area signature graded west (lower) to east (higher) within the North Central region (Fig. 3), concurrent  
357 with the aridity gradient within the region (Fig. 1). The two low flow signatures had a significant, but weaker  
358 correlation with one another ( $R = 0.71$ ,  $p < 0.01$ ).

359 The DryMonth/area was significantly correlated with many more independent variables than the baseflow  
360 index. Like the peak flow signatures, DryMonth/area was positively correlated with greater annual precipitation and  
361 water demand (P-ET) and negatively correlated with greater aridity (ET/P). The DryMonth/area was also positively  
362 correlated with total inundation within the floodplain, seasonally inundated area within the floodplain, and temporarily  
363 inundated area outside of the floodplain. No significant correlations, in contrast, were found with topographic or  
364 wetland variables (Table 4). The DryMonth/area had the greatest model explanatory power, relative to the other  
365 hydrologic signature models (Table 5). However, despite significant ( $p < 0.01$ ) correlations with remotely sensed  
366 inundation dynamics, there was no model improvement as landscape variables were added between the  $M_{\text{Climate}}$  and  
367  $M_{\text{All}}$  models (Table 5). The DryMonth/area was best explained by watershed aridity and annual precipitation. Further,  
368 the  $M_{\text{Climate}}$  model showed significant spatial autocorrelation within the residuals so that a residual autocovariate was  
369 included in the model and had a strong variable importance value (Table 6). This suggests that the DryMonth/area  
370 model would benefit from the addition of an independent variable, not yet identified in the analysis.

371 The baseflow index was negatively significantly ( $p < 0.01$ ) correlated with precipitation CV,  
372 evapotranspiration, and fraction of clay (Table 4). Adding landscape variables, unlike DryMonth/area, improved the  
373 baseflow index model by 5.43% (Table 5), and improved the relationship between the observed and predicted baseflow  
374 index values (Fig. 5b). While the precipitation CV was the most important variable in both the baseflow index  $M_{\text{All}}$   
375 and  $M_{\text{Climate}}$  models, the  $M_{\text{All}}$  model's improvement was entirely attributable to the inclusion of the amount of non-  
376 floodplain area classified as semi-permanent to permanent (i.e., large wetlands and lakes outside of the floodplain)  
377 (Table 6).



378  
379  
380  
381

**Figure 3.** Hydrological signature values by watershed including (a) flashiness index, (b) wet season flashiness index, (c) MAX30/area ( $\text{m}^3/\text{sec}/\text{km}^2$ ), (d) (Q10-Q95)/area ( $\text{m}^3/\text{sec}/\text{km}^2$ ), (e) DryMonth/area ( $\text{m}^3/\text{sec}/\text{km}^2$ ), and (f) baseflow index.



382 **Table 4.** Spearman correlation values between hydrologic signatures and variables. Significance ( $p < 0.01$ ) correlations,  
 383 after Bonferroni correction was applied, is shown in shaded gray. CV: coefficient of variation, FP: floodplain, NFP:  
 384 non-floodplain, Prop: proportion, MAX: maximum, SP-P: semi-permanent and permanent

Variable Type	Variable	Flashiness Index	Flashiness (wet season)	MAX 30/area	(Q10-Q95)/area	DryMonth /area	Baseflow index
Climate	Precipitation (P)	0.06	0.01	0.86	0.87	0.68	0.16
	Evapotranspiration (ET)	0.43	0.32	0.18	0.14	-0.15	-0.47
	Aridity index (ET/P)	-0.03	-0.03	-0.84	-0.87	-0.84	-0.37
	Water demand (P - ET)	-0.03	-0.02	0.78	0.83	0.82	0.41
	Precipitation seasonality	0.17	0.26	0.01	-0.04	0.21	0.2
	Precipitation CV	0.34	0.33	-0.26	-0.38	-0.55	-0.62
	Temperature seasonality	-0.29	-0.18	-0.3	-0.28	-0.05	0.24
	Temperature CV	-0.4	-0.3	-0.31	-0.28	-0.06	0.3
Land cover	Forest	-0.14	-0.17	0.28	0.32	0.18	0.15
	Developed	0.22	0.18	0.62	0.6	0.62	0.18
	Cultivated crops	-0.16	-0.13	0.03	0.06	0.3	0.27
	Stream density	0.36	0.29	0.37	0.35	-0.06	-0.33
Sub-surface	Clay fraction	0.4	0.37	0.25	0.15	-0.12	-0.44
	Sand fraction	-0.23	-0.27	-0.32	-0.26	-0.07	0.16
	Average soil thickness	-0.29	-0.3	0.14	0.18	0.32	0.2
	Water table depth	0.12	0.13	-0.54	-0.55	-0.45	-0.09
Topography	Slope	0.13	0.13	-0.23	-0.22	-0.27	0
	Elevation range	0.12	0.03	0.24	0.24	0.14	-0.04
	Topographic diversity	0.11	0.11	-0.17	-0.15	-0.2	0.04
Inundation Dynamics	Temporarily flooded, FP	0.27	0.23	0.42	0.40	0.24	-0.05
	Temporarily inundated, NFP	-0.06	-0.03	0.49	0.51	0.58	0.30
	Seasonally inundated, FP	-0.12	-0.15	0.66	0.69	0.59	0.15
	Seasonally inundated, NFP	-0.21	-0.19	0.36	0.37	0.39	0.14
	SP-P inundated, FP	-0.44	-0.46	0.24	0.33	0.33	0.14
	SP-P, inundated, NFP	-0.34	-0.32	0.13	0.11	0.13	0.04
	Total inundation, FP	-0.12	-0.15	0.60	0.63	0.52	0.12
Total inundation, NFP	-0.19	-0.17	0.37	0.37	0.41	0.17	
Wetland	Geographically Isolated Wetlands (GIW)	-0.31	-0.29	0.07	0.08	0.13	0.04
	Prop. of wetland area identified as GIW	-0.08	-0.05	0.08	0.03	0.06	0.01
	Floodplain	-0.02	-0.07	0.49	0.51	0.39	0
	National Wetland Inventory wetlands	-0.44	-0.44	0.12	0.19	0.28	0.19

385  
 386





387 **Table 5.** Model statistics for each hydrologic signature and version of the model including (1) climate variables only  
 388 ( $M_{Climate}$ ) and (2) all variables including wetland and surface water variables ( $M_{All}$ ). LOOCV: leave-one-out cross  
 389 validation, RMSE: root mean square error, AC: autocovariate, adj: adjusted, MAX: maximum

Signature	Model	$R^2$ (LOOCV)	$R^2$ adj. (LOOCV)	RMSE LOOCV)	Change in adj. $R^2$ from $M_{Climate}$ to $M_{All}$ (%)	Trees	Max. tree depth	Residual AC included	Variables selected
Flashiness index	$M_{Climate}$	0.501	0.474	0.254		700	4		3
	$M_{All}$	0.545	0.494	0.242	<b>4.28</b>	500	4	x	6
Flashiness index (wet season)	$M_{Climate}$	0.435	0.394	0.283		700	4		4
	$M_{All}$	0.482	0.434	0.271	<b>9.97</b>	700	4	x	5
MAX30/area	$M_{Climate}$	0.666	0.648	0.463		700	4		2
	$M_{All}$	0.699	0.665	0.439	<b>2.73</b>	700	4		6
(Q10-Q95)/area	$M_{Climate}$	0.753	0.730	0.007		500	3	x	5
	$M_{All}$	0.795	0.777	0.006	<b>6.31</b>	1000	4		5
DryMonth/area	$M_{Climate}$	0.838	0.820	0.001		700	4	x	6
	$M_{All}$	0.838	0.820	0.001	<b>0.00</b>	700	4	x	6
Baseflow index	$M_{Climate}$	0.576	0.545	0.118		1000	4		4
	$M_{All}$	0.603	0.574	0.114	<b>5.43</b>	1000	4		4

390



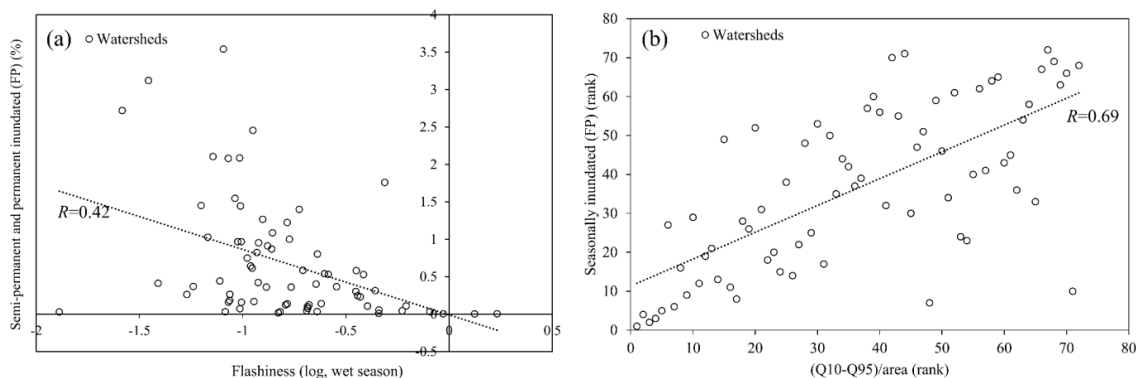
391 **Table 6.** Variable permutation importance of variables selected for  $M_{Climate}$ : model in which only climate variables  
 392 were considered, and  $M_{All}$ : all variables were considered, CV: coefficient of variation, min.: minimum, FP: floodplain,  
 393 NFP: non-floodplain, Q1, Q2, Q3, Q4: quartile, MAX: maximum, SP and P: semi-permanent and permanent

Variable Type	Variable	Flashiness index		Flashiness index (wet season)		MAX30/area		(Q10-Q95)/area		DryMonth/area		Baseflow index	
		$M_{Climate}$	$M_{All}$	$M_{Climate}$	$M_{All}$	$M_{Climate}$	$M_{All}$	$M_{Climate}$	$M_{All}$	$M_{Climate}$	$M_{All}$	$M_{Climate}$	$M_{All}$
Climate	Precipitation (P)			0.22		0.65	0.36	0.38	0.4	0.15	0.15	0.12	
	Evapo-transpiration (ET)	0.38		0.35		0.35				0.06	0.06	0.28	0.26
	Aridity index (ET/P)					0.32	0.31			0.28	0.28		
	Water demand (P - ET)	0.35		0.22					0.33				
	Precipitation seasonality	0.27		0.21				0.09	0.09	0.06	0.06	0.18	0.15
	Precipitation coefficient of variation									0.11	0.11	0.42	0.39
	Temperature coefficient of variation		0.27		0.27			0.06	0.08				
Landcover	Forest						0.08						
	Developed												
	Stream density					0.13		0.11					
Sub-surface	Clay fraction					0.06							
	Sand fraction		0.12										
	Annual minimum depth to water table		0.25		0.27								
Topography	Slope		0.12		0.16								
Inundation Dynamics	SP and P inundated, FP		0.24		0.3								
	SP and P inundated, NFP												0.2
	Temporarily flooded, FP						0.06						
Other	Residual autocovariate		0		0			0.16		0.33	0.33		
Color Legend:		Q1 (0-25%)		Q2 (26-50%)		Q3 (51-75%)		Q4 (76-100%)					

394  
 395  
 396  
 397  
 398

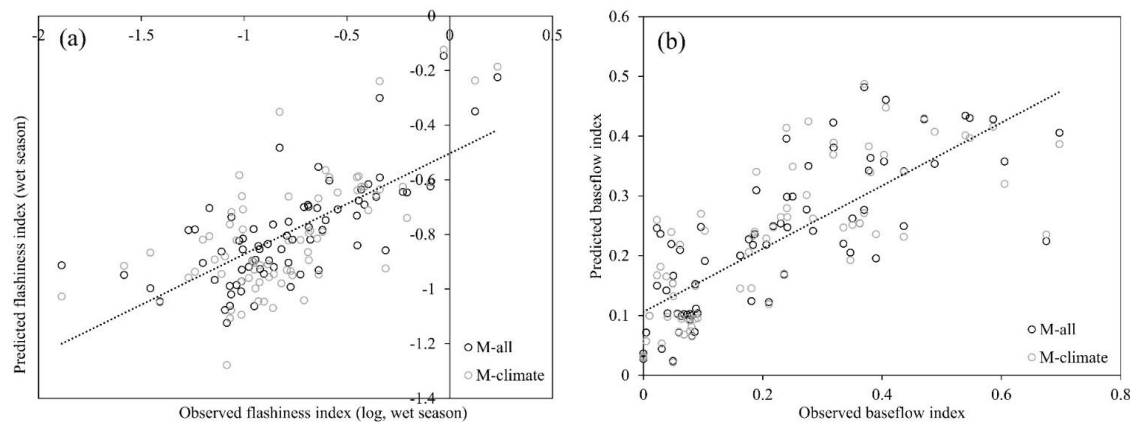


399



400  
401  
402  
403  
404  
405

**Figure 4.** Scatter plot of (a) wet season flashiness versus the percent of semi-permanent and permanent floodplain (FP) inundation, which was included in the  $M_{All}$ , and (b) (Q10-Q95)/area in relation to the percent of seasonally inundated. To match the Spearman correlation analysis, both variables in panel b were converted to rank. FP: floodplain



406  
407  
408

**Figure 5.** Scatter plots showing observed versus predicted with the  $M_{climate}$  and  $M_{all}$  models for (a) flashiness (wet season, unitless) and (b) baseflow index (unitless).



409 **4. Discussion**

410 **4.1 Role of climate**

411 Climate variables often provide the highest predictive power for many hydrologic signatures (Beck et al.,  
412 2015; McMillan et al., 2021). Similarly, in our analysis, climate variables showed the greatest variable importance  
413 within most of the models, especially in the high flow and low flow hydrologic signature models. The climate variables  
414 selected in the random forest models were generally consistent with variables in other studies exploring processes  
415 underlying hydrological signatures. Processes generating high discharge and flooding are variable across the United  
416 States (Berghuis et al., 2016), but rainfall and snowmelt (Jiang et al., 2022), as well as aridity (Sauquet et al., 2021),  
417 have been found to account for most peaks in discharge. Similarly, in our effort, annual precipitation, followed by  
418 aridity or water demand, had the greatest variable importance in predicting both seasonal peaks in discharge (i.e.,  
419 MAX30/area) as well as the difference between baseflow and high flow conditions (i.e., (Q10-Q95)/area). For the low  
420 flow signatures, annual evapotranspiration was selected for both DryMonth/area and the baseflow index, and the  
421 baseflow index was negatively significantly correlated with annual evapotranspiration, a finding consistent with Beck  
422 et al. (2013) and van Dijk (2010). Several studies have also related low flow metrics to precipitation (e.g., Small, 2006,  
423 Kelly and White, 2016). Consistent with this finding, for both the  $M_{Climate}$  and  $M_{All}$  baseflow index models,  
424 precipitation variability was an important variable.

425 **4.2 Role of surface water inundation**

426 There are still opportunities to incorporate new watershed descriptors that may improve the characterization  
427 of flow signatures (Gnann et al., 2020). Specifically, McMillan et al. (2021) argued that novel relationships may be  
428 discovered where hydrology is more important than climate. For example, flood signatures have been predicted using  
429 watershed drainage patterns (Oppel & Schumann, 2020), and surface waterbodies have been found to help predict  
430 baseflow signatures (Beck et al., 2013). More generally, the influence of a watershed's landscape, including vegetation  
431 type (Trancoso et al., 2016; Addor et al., 2018), topography (Beck et al., 2015, and geology (Kuentz et al., 2017), on  
432 discharge has been well established. Therefore, it was unsurprising that in our analysis most of the hydrologic  
433 signatures, five of the six, showed an improvement in the model explanatory power, relative to using climate variables  
434 alone. However, novel to this study was that model improvement for four of the six hydrologic signatures—flashiness,  
435 wet season flashiness, MAX30/area, and the baseflow index—was attributable, at least in part, to the inclusion of a  
436 remotely sensed inundation dynamic variable. Model selection of remotely sensed inundation dynamic variables over  
437 existing wetland and floodplain dataset variables suggests that consideration of surface water hydroperiod, alongside  
438 landscape position, was more helpful in explaining these hydrologic signatures than static datasets representing the  
439 spatial extent of wetlands (e.g., NWI, GIW) and floodplains (e.g., 100-year floodplain). Additionally, five of the six  
440 hydrologic signatures were significantly correlated with one or more of the remotely sensed inundation dynamic  
441 variables. Although we acknowledge that the results could be influenced by watershed selection, watershed size, and  
442 hydrologic signatures included in the analysis (McMillan et al., 2021), an improved understanding of the potential  
443 influence of surface water storage, such as wetlands, on stream behavior can help support watershed management and  
444 guide surface water storage restoration efforts across landscapes (Walters and Babbar-Sebens, 2016).



445 While it is evident that lakes and wetlands can store and contribute water to river networks (Fritz et al., 2018;  
446 Lane et al., 2018), it is less clear if surface water storage across multiple watersheds and regions has a measurable  
447 impact on river discharge dynamics. In our analysis, we found that although baseflow was significantly correlated  
448 with very few independent variables, the improvement in the baseflow index model from  $M_{\text{Climate}}$  to  $M_{\text{All}}$  was entirely  
449 attributable to the addition of the semi-permanent to permanent non-floodplain inundation variable. This finding  
450 suggests that baseflow may be influenced by wetlands and lakes that persist during dry seasons and years and are  
451 external to the floodplain. Similarly, previous research within select watersheds has found that wetlands stabilize low  
452 flow conditions (McLaughlin et al., 2014; Ameli and Creed, 2017; Blanchette et al., 2019). Geographically isolated  
453 wetlands, specifically, can contribute to baseflow (Evenson et al., 2015) and contribute water to as well as from  
454 shallow groundwater, like a sponge (McLaughlin et al., 2014; Yeo et al., 2019).

455 Surface water inundation variables also helped explain the flashiness signatures. Flashiness signatures  
456 represent streamflow response to high rainfall and snowmelt events, where streams that rise and fall quickly are  
457 considered flashier than those that maintain a steadier flow (Hannaford and March, 2008). Both flashiness signatures  
458 were inversely and significantly related to semi-permanent to permanent inundation within the floodplain, i.e., the  
459 locations of large wetlands and lakes continuous with, adjacent to, or near the stream network. Semi-permanent to  
460 permanent inundation within the floodplain was also selected by both  $M_{\text{All}}$  models and had the greatest variable  
461 importance of all selected variables for the wet season flashiness  $M_{\text{All}}$  model. While non-floodplain wetlands decrease  
462 streamflow variability (Yeo et al., 2019) and reduce flashiness (McLaughlin et al., 2014) in select watersheds, our  
463 analysis suggests that floodplains may also provide inundation storage important to stabilizing flow, a finding that  
464 confirms an abundance of prior research (Fritz et al., 2018; Wohl, 2022), and supports resilience against watershed-  
465 scale hydrological disturbances (Lane et al., 2023). The importance of variables that tend to be correlated with patterns  
466 of inundation has been previously documented, such as topography which has been found to control flashiness in  
467 streams across Europe (Kuentz et al., 2017), and soil moisture, which has been found to be helpful in explaining flood  
468 generation (Berghuijs et al., 2016) and the runoff coefficient (Trancoso et al., 2016). Yet, our flashiness findings were  
469 novel as most high flow signatures have not yet explicitly tested inundation-related, observation-based variables.

#### 470 **4.3 Challenges and limitations**

471 Even when incorporating novel, remotely sensed inundation data, characterizing the potential influence of  
472 surface water storage on river discharge is challenging (Golden et al., 2021). In our analyses, river discharge and  
473 surface water extent were significantly related to climate variables, including like precipitation (+), evapotranspiration  
474 (-), and aridity (-) (Song et al., 2018; Tulbure and Broich, 2019; Xia et al., 2019). Therefore, a correlation between  
475 surface water extent and river discharge may not necessarily be indicative of an interaction or influence and may  
476 simply suggest they are driven by the same climate forcing functions. For instance, in our analysis, watersheds with  
477 large seasonal peaks in discharge,  $\text{MAX}_{30}/\text{area}$  and  $(\text{Q}_{10}-\text{Q}_{95})/\text{area}$ , also tended to co-occur, or be significantly  
478 correlated with, watersheds that contained more floodplain and greater temporary and seasonal inundation. Yet, it is  
479 still unclear if the seasonal flooding acts to reduce or otherwise impact the peak discharge amount. Process-based  
480 hydrologic models can therefore potentially be used to complement statistical analyses and to help distinguish between



481 correlation and causality. For example, large wetlands have been shown to reduce storm-induced discharge peaks  
482 using a semi-distributed process-based watershed model (SWAT; Evenson et al., 2018). Further, discharge simulations  
483 for 96 watersheds across the globe demonstrated that surface water storage in wetlands reduced peak flows (Stacke  
484 and Hagemann, 2012). However, process-based hydrologic models are typically developed for a single or series of  
485 nested watersheds (Jones et al., 2019), limiting our ability to compare geographically disparate watersheds.  
486 Hydrological signatures, conversely, can facilitate the rapid comparison of many different, diverse watersheds.

487 A related challenge is deciphering the relative importance of environmental variables when they are highly  
488 correlated with another. Temporal variability in surface water extent, for instance, is a function of climate inputs,  
489 topography, and sub-surface characteristics (Heimhuber et al., 2016; Hayashi et al., 2016; Vanderhoof et al., 2018),  
490 making it difficult to clearly identify the influence of wetland and surface water inundation variables from other  
491 landscape variables. For example, in our study, slope was highly correlated (Spearman  $R > 0.7$ ) with seasonal, semi-  
492 permanent to permanent and total non-floodplain inundation variables, and the amount of temporary and seasonal  
493 non-floodplain inundation variables were significantly correlated with watershed aridity and water demand (Table  
494 A4). Therefore, while a forward selection process, guided by reduction in the RMSE, was used to select model  
495 variables, there could be some uncertainty in the model selection of one variable over another. In other cases,  
496 correlations between the inundation dynamic variables and previously available datasets can provide insights on the  
497 potential value-add of new independent variables. For example, while the NWI wetland dataset had a high correlation  
498 with semi-permanent and permanent inundation ( $R = 0.86$  and  $R = 0.81$ , for floodplain and non-floodplain, respectively),  
499 weaker correlations were observed with temporary and seasonal patterns of inundation (Table A4). Additionally, while  
500 surface water extent was used to represent surface water storage, the two are distinct measurements, and in the future,  
501 conversion of surface water (2D) to storage (3D) will facilitate improved modeling of total water distribution.

#### 502 **4.4 Management implications**

503 Hydrologic signatures have been used to support watershed management. For example, signatures related to  
504 flow magnitude, high flow frequency and flow variability have applications for flood management (Mogollon et al.,  
505 2016), wildlife habitat condition (Lowe et al., 2019), and riparian vegetation (Richter et al., 1996). Further, changes  
506 in hydrologic signatures over time have been used to examine the impacts of management actions or to assess a  
507 watershed's vulnerability or resilience to change (Hannaford and Marsh, 2008; Mogollon et al., 2016; McMillan et  
508 al., 2021; Lane et al., 2023).

509 Applying results linking different watershed characteristics (e.g., climate, land use, geology) to hydrologic  
510 signature variability can therefore help inform future watershed management actions. However, a challenge is how to  
511 synthesize this information in a useful way (Gnann et al., 2020). One approach would be to focus on managing  
512 watershed characteristics that are highly correlated with a pre-determined flow signature target (e.g., those associated  
513 with flood risks). For example, in our analyses, the association of greater semi-permanent and permanent floodplain  
514 inundation with less flashiness suggests that protection and restoration of floodplains may be particularly important  
515 in watersheds with flashy discharge. On the other hand, we found that non-floodplain surface water inundation helped  
516 explain the variability in the baseflow index, which describes the proportion of flow coming from groundwater, and



517 by inference the relative potential vulnerabilities for drought and extreme low flow conditions. Results from our  
518 analyses—and other future analyses leveraging large satellite-based data sets against streamflow records—can therefore  
519 advance our ability to support improved watershed management, e.g., in the face of future floods and drought  
520 (Winsemius et al., 2016; Stewart et al., 2020).

## 521 **5. Conclusion**

522 Here we demonstrate that in addition to the insights hydrologic signatures provide about process-based  
523 streamflow dynamics (Addor et al., 2018; McMillian, 2019), they can also be used to assess the potential influence of  
524 surface water inundation dynamics on river discharge. While climate variables represented the dominant explanatory  
525 variables, additional variables, in particular the novel, remotely sensed inundation dynamics, also contributed to  
526 explaining variability in many of the hydrologic signatures. Five of the six flow signatures, or all except the baseflow  
527 index, were significantly correlated with surface water inundation dynamic variables, and four of the six signature  
528 models that included all variables included surface water inundation dynamics as significant variables. Our models  
529 suggest that increased floodplain inundation co-occurs with decreased streamflow flashiness and higher peak flows.  
530 These results highlight the importance of protecting and restoring surface water storage capacities within floodplains.  
531 Additionally, our model results suggest that protection and restoration of non-floodplain wetlands could potentially  
532 benefit baseflow conditions—and thereby minimize or moderate drought and low flow extremes. The study further  
533 underscores that managing risks and watershed resilience associated with high and low flow river conditions may  
534 require consideration of watershed-wide surface water storage dynamics.

## 535 **Data Availability**

536 Data archiving is currently underway, and the surface water data produced for this analysis will be available for  
537 download in the U.S. Geological Survey ScienceBase Data Catalog concurrent with the manuscript publication.

## 538 **Author Contribution**

539 MV, PN, HG, CL and JC contributed to the work's conception. PN, WK, and MV contributed to data processing and  
540 analysis. MV, PW, HE, CL, JC, WK and WD contributed to the interpretation of the results as well as the writing and  
541 editing.

## 542 **Competing Interests**

543 The authors declare that they have no conflicts of interest.



#### 544 Acknowledgements

545 This research was funded by the U.S. Geological Survey’s National Land Imaging and Land Change Science Programs  
546 and the U.S. Environmental Protection Agency’s, Office of Research and Development through an interagency  
547 agreement (DW-014-92569201-0, “Multisource remote sensing to enhance national mapping of aquatic resources”).  
548 We appreciate comments on earlier versions from Brent Johnson and Kyle McLean. We also appreciate support from  
549 Jeremy Havens and Kylen Solvik. Any use of trade, firm, or product names is for descriptive purposes only and does  
550 not imply endorsement by the U.S. Government. This publication represents the views of the authors and does not  
551 necessarily reflect the views or policies of the U.S. EPA.

#### 552 References

- 553 Abatzoglou J. T.: Development of gridded surface meteorological data for ecological applications and modelling, *Int.*  
554 *J. Climatol.*, 33(1), 121-131, 2013.
- 555 Addor, N., Nearing, G., Prieto, C., Newman, A. J., Le Vine, N., and Clark, M. P.: A ranking of hydrological signatures  
556 based on their predictability in space, *Water Resour. Res.*, 54, 8792–8812, 2018.
- 557 Ameli, A. A. and Creed, I. F.: Quantifying hydrologic connectivity of wetlands to surface water systems, *Hydrol.*  
558 *Earth Syst. Sc.*, 21, 1791–808, 2017.
- 559 Ameli, A. A. and Creed, I. F.: Does wetland location matter when managing wetlands for watershed-scale flood and  
560 drought resilience? *J. Am. Water Resour. As.*, 55, 529–542, 2019.
- 561 Apurv, T. and Cai, X.: Regional drought risk in the contiguous United States, *Geophys. Res. Lett.*, 48(5),  
562 e2020GL092200, 2021.
- 563 Baker, D. B., Richards, R. P., Loftus, T. T., and Kramer, J. W.: A new flashiness index: Characteristics and  
564 applications to midwestern rivers and streams, *J. Am. Water Resour. As.*, 40(2), 503-522, 2004.
- 565 Beck, H. E., de Roo, A. and van Dijk, A. I. J. M.: Global maps of streamflow characteristics based on observations  
566 from several thousand catchments, *J. Hydrometeorol.*, 16, 1478-1501, 2015.
- 567 Beck, H. E., van Dijk, A. I. J. M., Miralles, D. G., de Jeu, R. A. M., Bruijnzeel, L. A., McVicar, T. R., and Schellekens,  
568 J.: Global patterns in base flow index and recession based on streamflow observations from 3394 catchments,  
569 *Water Resour. Res.*, 49, 7843-4863, 2013.
- 570 Berghuijs, W. R., Woods, R. A., Hutton, C. J., and Sivapalan, M.: Dominant flood generating mechanisms across the  
571 United States, *Geophys. Res. Lett.*, 43, 4382-4390, 2016.
- 572 Betts, M. G., Diamond, A. W., Forbes, G. J., Villard, M. -A., and Gunn, J. S.: The importance of spatial  
573 autocorrelation, extent and resolution in predicting forest bird occurrence, *Ecol. Model.*, 191(2), 197-224, 2006.
- 574 Blanchette, M., Rousseau, A. N., Foulon, É., Savary, S., and Poulin, M.: What would have been the impacts of  
575 wetlands on low flow support and high flow attenuation under steady state land cover conditions? *J. Environ.*  
576 *Manage.*, 234, 448–457, 2019.
- 577 Budyko, M.: *The Heat Balance of the Earth’s Surface*. Washington, DC: Springer, 1958.
- 578 Bullock, A., Acreman, M.: The role of wetlands in the hydrological cycle, *Hydrol. Earth Syst. Sc.*, 7, 358-389, 2003.
- 579 Cawley, G. C. and Talbot, N. L. C.: On over-fitting in model selection and subsequent selection bias in performance  
580 evaluation, *J. Mach. Learn. Res.*, 11, 2079-2107, 2010.
- 581 Cowardin, L. M., Carter, and F. C., Golet, E. T.: Classification of wetlands and deepwater habitats of the United States.  
582 United States Department of the Interior, Fish and Wildlife Service, Washington, D.C., USA, 1979.
- 583 Daigle, A., St-Hilaire, A., Beveridge, D., Caissie, D., and Benyahya, L.: Multivariate analysis of the low-flow regimes  
584 in eastern Canadian rivers, *Hydrolog. Sci. J.*, 56, 51-67, 2011.
- 585 Donnelly, J. P., Naugle, D. E., Collins, D. P., Dugger, B. D., Allred, B. W., Tack, J. D., and Dreitz, V. J.: Synchronizing  
586 conservation to seasonal wetland hydrology and waterbird migration in semi-arid landscapes, *Ecosphere*, 10(6),  
587 e02758, 2019.
- 588 Eamus, D., Hatton, T., Cook, P., and Colvin, C.: *Ecologyhydrology: vegetation function, water and resource management*,  
589 CSIRO Publishing, Australia, 360 pp, 2006.
- 590 Emerson, R. W.: Bonferroni correction and type I error., *J. Vis. Impair. Blind.*, 114(1), 77-78, 2020.





- 591 Evenson, G. R., Golden, H. E., Lane, C. R., and D'Amico, E.: Geographically isolated wetlands and watershed  
592 hydrology: A modified model analysis, *J. Hydrol.*, 529, 240–256, 2015.
- 593 Evenson, G. R., Jones, C. N., McLaughlin, D. L., Golden, H. E., Lane, C. R., DeVries, B., Alexander, L. C., Lang, M.  
594 W., McCarty, G. W., and Sharifi, A.: A watershed-scale model for depressional wetland-rich landscapes, *J.*  
595 *Hydrol. X.* 1, 100002, 2018.
- 596 Falcone, J.: GAGES-II: Geospatial attributes of gages for evaluating streamflow. U.S. Geological Survey, Reston,  
597 Virginia, [https://water.usgs.gov/lookup/getspatial?gagesII\\_Sept2011](https://water.usgs.gov/lookup/getspatial?gagesII_Sept2011) (last accessed April 1, 2024), 2011.
- 598 Fritz, K. M., Schofield, K. A., Alexander, L. C., McManus, M. G., Golden, H. E., Lane, C. R., Kepner, W. G., LeDuc,  
599 S. D., DeMeester, J. E., and Pollard, A. I.: Physical and chemical connectivity of streams and riparian wetlands  
600 to downstream waters: a synthesis, *J. Am. Water Resour. As.*, 54(2), 323–345, 2018.
- 601 Gesch, D., Oimoen, M., Greenlee, S., Nelson, C., Steuck, M., and Tyler, D.: The national elevation dataset,  
602 *Photogramm. Eng. Rem. S.*, 68(1), 5–11, 2002.
- 603 Gnann, S., McMillan, H., Woods, R., and Howden, N.: Including regional knowledge improves baseflow signature  
604 predictions in large sample hydrology, *Water Resour. Res.*, 57(2), e2020WR028354, 2021.
- 605 Golden, H. E., Lane, C. R., Amatya, D. M., Bandilla, K. W., Raanan Kiperwas, H., Knightes, C. D., and Ssegane, H.:  
606 Hydrologic connectivity between geographically isolated wetlands and surface water systems: a review of  
607 select modeling methods, *Environ. Modell. Softw.*, 53, 190–206, 2014.
- 608 Golden, H. E., Lane, C. R., Rajib, A., and Wu, Q.: Improving global flood and drought predictions: integrating non-  
609 floodplain wetlands into watershed hydrologic models, *Environ. Res. Lett.*, 16, 091002, 2021.
- 610 Gregorutti, B., Michel, B., and Saint-Pierre, P.: Correlation and variable importance in random forests, *Stat. Comput.*,  
611 27, 659–678, 2016.
- 612 Hannaford, J. and Marsh, T.: High-flow and flood trends in a network of undisturbed catchments in the UK, *Int. J.*  
613 *Climatol.*, 28, 1325–1338, 2008.
- 614 Hastie, T., Tibshirani, R. and Friedman, J.: *The Elements of Statistical Learning*, Springer, New York, 2009.
- 615 Hayashi, M., van der Kamp, G., and Rosenberry, D. O.: Hydrology of prairie wetlands: Understanding the integrated  
616 surface-water and groundwater processes, *Wetlands*, 36, 237–254, 2016.
- 617 Heidari, H., Arabi, M., Warziniack, T., and Kao, S. C.: Assessing shifts in regional hydroclimatic conditions of U.S.  
618 river basins in response to climate change over the 21<sup>st</sup> century, *Earth's Future*, 8(10), e2020EF001657, 2020.
- 619 Heimhuber, V., Tulbure, M. G., and Broich, M.: Modeling 25 years of spatio-temporal surface water and inundation  
620 dynamics on large river basin scale using time series of Earth observation data, *Hydrol. Earth Syst. Sc.*, 20(6),  
621 2227–2250, 2016.
- 622 Hendry, A., Haigh, I. D., Nicholls, R. J., Winter, H., Neal, R., Wahl, T., Joly-Laugel, A., and Darby, S. E.: Assessing  
623 the characteristics and drivers of compound flooding events around the UK coast, *Hydrol. Earth Syst. Sc.*, 23,  
624 3117–3139, 2019.
- 625 Hengl, T., Nussbaum, M., Wright, M. N., Heuvelink, G. B. M., and Gräler, B.: Random forest as a generic framework  
626 for predictive modeling of spatial and spatio-temporal variables, *PeerJ*, e5518, 2018.
- 627 Homer, C., Dewitz, J., Jin, S., Xian, G., Costello, C., Danielson, P., Gass, L., Funk, M., Wickham, J., Stehman, S.,  
628 Auch, R., and Riitters, K.: Conterminous United States land cover change patterns 2001–2016 from the 2016  
629 National Land Cover Database, *ISPRS J. Photogramm.*, 162, 184–199, 2020.
- 630 Jiang, S., Zheng, Y., Wang, C., and Babovic, V.: Uncovering flooding mechanisms across the contiguous United  
631 States through interpretive deep learning on representative catchments, *Water Resour. Res.*, 58(1),  
632 e2021WR030185, 2022.
- 633 Jones, N. C., Ameli, A., Neff, B. P., Evenson, G. R., McLaughlin, D. L., Golden, H. E., and Lane, C. R.: Modeling  
634 connectivity of non-floodplain wetlands: insights, approaches, and recommendations, *J. Am. Water Resour.*  
635 *As.*, 55, 559–577, 2019.
- 636 Kelly, V.J., and White, S.: A method for characterizing late-season low-flow regime in the upper Grand Ronde River  
637 Basin, Oregon. U.S. Geological Survey Scientific Investigations Report 2016-5041, 2016.
- 638 Kennard, M. J., Mackay, S. J., Pusey, B. J., Olden, J. D., and Marsh, N.: Quantifying uncertainty in estimation of  
639 hydrologic metrics for ecohydrological studies, *River Res. Appl.*, 26, 137–156, 2010.
- 640 Kuentz, A., Arheimer, B., Hundecha, Y., and Wagener, T.: Understanding hydrologic variability across Europe  
641 through catchment classification, *Hydrol. Earth Syst. Sc.*, 21, 2863–2879, 2017.
- 642 Klute, D., Lovallo, M., and Tzilkowski, W.: Autologistic regression modeling of American woodcock habitat use with  
643 spatially dependent data. In: Scott, J.M., Heglund, P.J., Morrison, M.L., Haufler, J.B., Raphael, M.G., Wall,  
644 W.A., Sampson, F.B. (Eds.), *Predicting Species Occurrences, Issues of Accuracy and Scale*. Island Press,  
645 Washington, pp. 335–343, 2002.



- 646 Kuppel, S., Houspanossian, J., Nosoetto, M. D., and Jobbágy, E. G.: What does it take to flood the Pampas? Lessons  
647 from a decade of strong hydrological fluctuations, *Water Resour. Res.*, 51, 2937–2950, 2015.
- 648 Lane, C. R. and D’Amico, E.: Identification of putative geographically isolated wetlands of the conterminous United  
649 States, *J. Am. Water Resour. As.*, 52 705–22, 2016.
- 650 Lane, C. R., Leibowitz, S. G., Autrey, B. C., LeDuc, S. D., and Alexander, L. C.: Hydrological, physical, and chemical  
651 functions and connectivity of non-floodplain wetlands to downstream waters: a review, *J. Am. Water Resour.*  
652 *As.*, 54(2), 346–371, 2018.
- 653 Lane, C. R., Creed, I. F., Golden, H. E., Leibowitz, S. G., Mushet, D. M., Rains, M. C., Wu, Q., D’Amico, E.,  
654 Alexander, L. C., Ali, G. A., Basu, N. B., Bennett, M. G., Christensen, J. R., Cohen, M. J., Covino, T. P.,  
655 DeVries, B., Hill, R. A., Jensco, K., Lang, M. W., McLaughlin, D., Rosenberry, D. O., Rover, J., and  
656 Vanderhoof, M. K.: Vulnerable waters are essential to watershed resilience, *Ecology*, 26, 1–28, 2022.
- 657 Leibowitz, S. G.: Geographically isolated wetlands: Why we should keep the term, *Wetlands*, 35, 997–1003, 2015.
- 658 Lowe, W. H., Swartz, L. K., Addis, B. R., and Likens, G. E.: Hydrologic variability contributes to reduced survival  
659 through metamorphosis in a stream salamander, *Proc. Natl. Acad. Sci.*, 116(39), 19563–19570, 2019.
- 660 McLaughlin, D. L., Kaplan, D. A., and Cohen, M. J.: A significant nexus: geographically isolated wetlands influence  
661 landscape hydrology, *Water Resour. Res.*, 50, 7153–66, 2014.
- 662 McMillan, H.: Linking hydrologic signatures to hydrologic processes: a review, *Hydrol. Process.*, 34(6), 1393–1409,  
663 2019.
- 664 McMillan, H. K.: A review of hydrologic signatures and their applications, *WIREs Water*, 8(1), doi:  
665 10.1002/wat2.1499, 2021.
- 666 Mehdiipoor, H., Zurita-Milla, R., Izquierdo-Verdiguier, E., and Betancourt, J. L.: Influence of source and scale of  
667 gridded temperature data on modelled spring onset patterns in the conterminous United States, *Int. J. Climatol.*,  
668 38(14), 5430–5440, 2018.
- 669 Mogollon, B., Frimpong, E. A., Hoegh, A. B., and Angermeier, P. L.: Recent changes in stream flashiness and  
670 flooding, and effects of flood management in North Carolina and Virginia, *J. Am. Water Resour. As.*, 52, 561–  
671 577, 2016.
- 672 Murphy, M. A., Evans, J. S., and Storfer, A.: Quantifying *Bufo boreas* connectivity in Yellowstone National Park with  
673 landscape genetics, *Ecology*, 91, 252–261, 2010.
- 674 National Atlas of the United States: Major Dams of the United States, Puerto Rico and the US Virgin Islands.  
675 Delivered by ArcGIS online (last accessed September 6, 2022), 2006.
- 676 National River Flow Archive: Derived flow statistics. Available online: <https://nrfa.ceh.ac.uk/derived-flow-statistics>  
677 (last accessed April 1, 2024), 2024.
- 678 NOAA: U.S. Billion-dollar weather and climate disasters, National Oceanic and Atmospheric Administration  
679 (NOAA), National Centers for Environmental Information, <https://doi.org/10.25921/stkw-7w73>.
- 680 Oppel, H., and Schumann, A. H.: Machine learning based identification of dominant controls on runoff dynamics,  
681 *Hydrol. Process.*, 34, 2450–2465, 2020.
- 682 Oueslati, O., De Girolamo, A. M., Abouabdillah, A., Kjeldsen, T. R., and Lo Porto, A.: Classifying the flow regimes  
683 of Mediterranean streams using multivariate analysis, *Hydrol. Process.*, 29, 4666–4682, 2015.
- 684 Pedregosa, F., Varoquaux, G., Gramfort, A., Michel, V., Thirion, B., Grisel, O., Blondel, M., Prettenhofer, P., Weiss,  
685 R. and Dubourg, V.: Scikit-learn: Machine learning in Python, *J. Mach. Learn. Res.*, 12, 2825–2830, 2011.
- 686 Rains, M. C., Leibowitz, S. G., Cohen, M. J., Creed, I. F., Golden, H. E., Jawitz, J. W., Kalla, P., Lane, C. R., Lang,  
687 M. W., and McLaughlin, D. L.: Geographically isolated wetlands are part of the hydrological landscape,  
688 *Hydrol. Process.*, 30(1), 153–160, 2016.
- 689 Rajib A., Golden H. E., Lane, C. R., and Wu, Q.: Surface depression and wetland water storage improves major river  
690 basin hydrologic predictions, *Water Resour. Res.*, 56, e2019WR026561, 2020.
- 691 Richter, B. D., Baumgartner, J. V., Powell, J., and Braun, D. P.: A method for assessing hydrologic alteration within  
692 ecosystems, *Conserv. Biol.*, 10, 1163–1174, 1996.
- 693 Sauquet, E., Shanafield, M., Hammond, J. C., Sefton, C., Leigh, C., and Datry, T.: Classification and trends in  
694 intermittent river flow regimes in Australia, northwestern Europe, and USA: A global perspective, *J. Hydrol.*,  
695 597, 126170, 2021.
- 696 Scott, D. T., Gomez-Velez, J. D., Jones, C. N., and Harvey, J. W.: Floodplain inundation spectrum across the United  
697 States, *Nat. Commun.*, 10, 5194, 2019.
- 698 Shaw, D. A., Vanderkamp, G., Conly, F. M., Pietroniro, A., and Martz, L.: The fill-spill hydrology of prairie wetland  
699 complexes during drought and deluge, *Hydrol. Process.*, 26, 3147–3156, 2012.
- 700 Sherrouse, B.C. and Hawbaker, T.J.: HOPS: Hyperparameter optimization and predictor selection v1.0, U.S.  
701 Geological Survey Software Release, <https://doi.org/10.5066/P9P81HUR>, 2023.



- 702 Small, D.: Trends in precipitation and streamflow in the eastern U.S.: Paradox or perception? *Geophys. Res. Lett.*, 33,  
703 L03403, 2006.
- 704 Song, C., Ke, L., Pan, H., Zhan, S., Liu, K., and Ma, R.: Long-term surface water changes and driving cause in Xiong-  
705 an, China: from dense Landsat time series images and synthetic analysis, *Sci. Bull.*, 63(11), 708-716, 2018.
- 706 Stacke, T. and Hagemann, S.: Development and evaluation of a global dynamical wetlands extent scheme, *Hydrol.*  
707 *Earth Syst. Sc.*, 16, 2915-2933, 2012.
- 708 Stepchinski, L. M., Rains, M. C., Lee, L. C., Lis, R. A., Nutter, W. L., Rains, K. C., and Stewart, S. R.: Hydrologic  
709 connectivity and flow generation from California vernal pool, swale, and headwater stream complexes to  
710 downstream waters, *Wetlands*, 43, 34, 2023.
- 711 Stewart, I. T., Rogers, J., and Graham, A.: Water security under severe drought and climate change: Disparate impacts  
712 of the recent severe drought on environmental flows and water supplies in Central California, *J. Hydrol.* X, 7,  
713 100054, 2020.
- 714 Theobald, D. M., Harrison-Atlas, D., Monahan, W. B., and Albano, C. M.: Ecologically-relevant maps of landforms  
715 and physiographic diversity for climate adaptation planning, *PLoS ONE*, 10(12), e0143619, 2015.
- 716 Thornton, M. M., Shrestha, R., Wei, Y., Thornton, P. E., Kao, S., Wilson, B. E.: Daymet: Daily Surface Weather Data  
717 on a 1-km Grid for North America, Version 4. ORNL DAAC, Oak Ridge, Tennessee,  
718 USA. <https://doi.org/10.3334/ORNLDAAAC/1840>, 2020.
- 719 Trancoso, R., Phinn, S., McVicar, T. R., Larsen, J. R., McAlpine, C. A.: Regional variation in streamflow drivers  
720 across a continental climatic gradient, *Ecohydrology*, 10, e1816, 2016.
- 721 Tulbure, M. and Broich, M.: Spatiotemporal patterns and effects of climate and land use on surface water extent  
722 dynamics in a dryland region with three decades of Landsat satellite data, *Sci. Total Environ.*, 658, 1574-1585,  
723 2019.
- 724 USFS: U.S. Stream Flow Metric Dataset: Modeled metrics for stream segments in the United States under historical  
725 conditions and projected climate change scenarios. Data Guide. Boise, ID, U.S. Department of Agriculture,  
726 U.S. Forest Service (USFS), (Last accessed September 6, 2022), 2022.
- 727 USFWS: National Wetlands Inventory. U.S. Fish and Wildlife (USFWS)  
728 Service. <https://www.fws.gov/program/national-wetlands-inventory>. (Last accessed April 1, 2024), 2019.
- 729 USGS: High Resolution, National Hydrography Dataset, U.S. Geological Survey (USGS), The National Map,  
730 Hydrography, <https://apps.nationalmap.gov/services/> (Last accessed August 4, 2022), 2022.
- 731 USGS: U.S. Geological Survey water data for the Nation: U.S. Geological Survey (USGS) National Water  
732 Information System database, <https://doi.org/10.5066/F7P55KJN> (Last accessed (Last accessed April 1, 2024),  
733 2024).
- 734 Vabalas, A., Gowen, E., Poliakoff, E. and Casson, A. J.: Machine learning algorithm validation with a limited sample  
735 size, *PLoS ONE*, 14(11), e0224365, 2019.
- 736 van Dijk, A. I. J. M.: Climate and terrain factors explaining streamflow response and recession in Australian  
737 catchments, *Hydrol. Earth Syst. Sc.*, 14, 159-169, 2010.
- 738 Vanderhoof, M. K., Alexander, L. C., and Todd, M. J.: Temporal and spatial patterns of wetland extent influence  
739 variability of surface water connectivity in the Prairie Pothole Region, United States, *Landscape Ecol.*, 31(4),  
740 805-824, 2016.
- 741 Vanderhoof, M. K., Lane, C. R., McManus, M. G., Alexander, L. C., and Christensen, J. R.: Wetlands inform how  
742 climate extremes influence surface water expansion and contraction, *Hydrol. Earth Syst. Sc.*, 22(3), 1851-1873,  
743 2018.
- 744 Vanderhoof, M. K., Alexander, L., Christensen, J., Solvik, K., Nieuwlandt, P. and Sagehorn, M.: High-frequency time  
745 series comparison of Sentinel-1 and Sentinel-2 for open and vegetated water across the United States (2017-  
746 2021), *Remote Sens. Environ.*, 288, 113498, 2023.
- 747 Vanderhoof, M. K., Christensen, J. R., Alexander, L. C., Lane, C. R., and Golden, H. E.: Climate change will impact  
748 surface water extents across the central United States, *Earth's Future*, 12(2), e2023EF004106, 2024.
- 749 Walters, K. M., and Babbar-Sebens, M.: Using climate change scenarios to evaluate future effectiveness of potential  
750 wetlands in mitigating high flows in a Midwestern U.S. watershed, *Ecol. Eng.*, 89, 80-102, 2016.
- 751 Winsemius, H. C., Aerts, J. C. J. H., van Beek, L. P. H., Bierkens, M. F. P., Bouwman, A., Jongman, B., Kwadijk, J.  
752 C. J., Ligtoet, W., Lucas, P. L., van Vuuren, D. P., and Ward, P. J.: Global drivers of future river flood risk,  
753 *Nat. Clim. Change*, 6, 381-385, 2016.
- 754 Wohl, E.: An integrative conceptualization of floodplain storage, *Rev. Geophys.*, 59(2), e2020RG000724, 2021.
- 755 Woznicki, S. A., Baynes, J., Panlasigui, S., Mehaffey, M., and Neale, A.: Development of a spatially complete  
756 floodplain map of the conterminous United States using random forest, *Sci. Total Environ.*, 647, 942-953, 2019.



- 757 Wu, G., Chen, J., Shi, X., Kim, J. S., Xia, J., and Zhang, L.: Impacts of global climate warming on meteorological and  
758 hydrological droughts and their propagations, *Earth's Future*, 10(3), e2021EF002542, 2022.
- 759 Wu, Y., Zhang, G., Rousseau, A. N., Xu, Y. J. and Foulon, E.: On how wetlands can provide flood resilience in a  
760 large river basin: a case study in Nenjiang river Basin, China, *J. Hydrol.*, 587, 125012, 2020.
- 761 Xia, H., Zhao, J., Qin, Y., Yang, J., Cui, Y., Song, H., Ma, L., Jin, N., and Meng, Q.: Changes in water surface area  
762 during 1989-2017 in the Huai River Basin using Landsat Data and Google Earth Engine, *Remote Sens.*, 11(15),  
763 1824, 2019.
- 764 Yeo, I., Lee, S., Lang, M. W., Yetemen, O., McCarty, G. W., Sadeghi, A. M., and Evenson, G.: Mapping landscape-  
765 level hydrological connectivity of headwater wetlands to downstream waters: A catchment modeling approach  
766 – Part 2, *Sci. Total Environ.*, 653, 1557-1570, 2019.
- 767 Zeng, L., Shao, J., and Chu, X.: Improved hydrologic modeling for depression-dominated areas, *J. Hydrol.*, 590,  
768 125269, 2020.



769 **Appendix**

770 **Table A1.** The 72 U.S. Geological survey gages and watersheds included in the analysis. The 2016–2023 period is  
 771 shown relative to the Palmer Drought Severity Index (PDSI, 1980–2021). NHD: National hydrographic dataset, NWI:  
 772 National Wetland Inventory. CC: cultivated crops, DF: deciduous forest, D: developed, HP: hay/pasture, EF:  
 773 evergreen forest, WW: woody wetlands, MF: mixed forest, SS: shrub/scrub, H: herbaceous

Gage ID	Site ID	U.S. State(s)	Area (km <sup>2</sup> )	NHD Density (m km <sup>2</sup> )	NWI (% area)	PDSI (min, %)	PDSI (max, %)	PDSI (median, %)	Primary land cover
01491000	MD1	MD, DE	292	2030.7	28.6	32.6	100.0	66.5	CC (47%)
01578475	MD2	MD, PA	458	1069.2	2.6	6.1	100.0	72.4	CC (43%)
01580520	MD3	MD, PA	425	1130.1	2.1	8.9	100.0	67.4	DF (30%)
01594440	MD4	MD	907	1571.9	6.4	16.7	100.0	64.4	D (36%)
01643000	MD5	MD, PA	2112	1394.3	3.0	4.2	100.0	57.5	HP (27%)
02049500	VA1	VA	1583	1497.8	15.7	33.0	100.0	79.3	EF (29%)
02131500	SC1	SC, NC	1720	1451.6	10.3	18.3	100.0	53.7	EF (26%)
02135000	SC2	SC, NC	7256	1628.6	27.2	8.5	100.0	78.0	WW (31%), CC (31%)
02136000	SC3	SC	3211	1738.0	27.0	17.6	100.0	75.2	CC (32%), WW (31%)
02175000	SC4	SC	7077	1163.0	17.3	27.1	98.0	75.5	EF (25%), WW (24%)
02198000	GA1	GA	1676	1365.2	12.0	19.4	96.6	61.1	EF (26%)
02202500	GA2	GA	6887	1249.8	16.8	21.1	97.7	60.2	EF (26%)
05056000	ND1	ND	4862	283.9	10.6	1.2	100.0	56.3	CC (52%)
05057200	ND2	ND	1897	259.2	11.6	0.0	100.0	65.0	CC (67%)
05062500	MN1	MN	2407	745.9	23.9	3.4	100.0	58.6	CC (39%)
05066500	ND3	ND	3218	774.1	6.9	0.3	100.0	63.4	CC (81%)
05078500	MN2	MN	3518	862.3	23.5	1.2	100.0	54.5	CC (48%)
05090000	ND4	ND	1742	1068.9	3.7	1.5	100.0	51.0	CC (73%)
05123400	ND5	ND	3206	515.6	12.2	1.0	97.8	48.8	CC (48%)
05131500	MN3	MN	4384	608.9	42.4	4.5	100.0	84.4	WW (49%)
05132000	MN4	MN	3895	537.3	48.7	5.6	100.0	71.1	WW (49%)
05244000	MN5	MN	2683	471.2	23.8	0.9	100.0	52.3	DF (27%)
05300000	MN6	MN, SD	2468	1286.4	11.5	11.6	100.0	66.6	CC (68%)
05304500	MN7	MN	4899	733.6	17.0	4.8	100.0	62.5	CC (66%)
05313500	MN8	MN, SD	1801	1129.0	8.8	8.5	100.0	58.8	CC (80%)
05336700	MN9	MN	2252	676.5	34.1	17.0	100.0	87.8	WW (34%)
05388250	IA1	IA, MN	2010	1548.4	2.7	9.2	100.0	76.1	CC (61%)
05412500	IA2	IA	3858	1414.9	2.4	6.9	100.0	81.6	CC (66%)
05418500	IA3	IA	4019	1452.5	2.1	6.3	100.0	70.8	CC (69%)
05422000	IA4	IA, MN	6049	1248.5	4.6	5.9	99.7	70.2	CC (79%)
05434500	WI1	WI, IL	2677	1618.6	3.0	5.1	100.0	71.9	CC (44%)
05447500	IL1	IL	2576	1115.6	1.9	20.7	100.0	74.9	CC (85%)
06018500	MT1	MT	9373	1628.9	3.9	0.3	89.3	50.9	SS (47%)
06052500	MT2	MT, WY	4634	1376.2	2.9	1.2	97.4	61.8	EF (47%)
06076690	MT3	MT	2189	1695.3	4.3	1.4	98.1	62.7	H (35%)
06468170	ND6	ND	2809	302.6	7.4	1.0	100.0	66.3	CC (67%)
06471200	ND7	ND, SD	1869	627.2	11.2	1.2	100.0	70.8	CC (62%)
06479525	SD1	SD	2467	947.8	9.8	19.3	100.0	67.4	CC (59%)
06481500	SD2	SD	1604	1102.0	8.7	8.8	100.0	62.0	CC (72%)
06815000	NE1	NE, KS	3473	1688.2	1.8	4.1	99.2	52.8	CC (54%)
06821190	MO1	MO, IA	6179	1925.6	4.8	11.3	99.0	56.6	CC (50%)
06908000	MO2	MO	2895	1737.9	4.2	3.5	90.4	51.9	HP (38%)
06916600	KS2	KS, MO	8387	1685.9	3.8	12.3	100.0	57.5	HP (37%)
06918060	MO3	MO, KS	2773	1669.2	5.4	4.7	100.0	57.0	HP (56%)



Gage ID	Site ID	U.S. State(s)	Area (km <sup>2</sup> )	NHD Density (m km <sup>2</sup> )	NWI (% area)	PDSI (min, %)	PDSI (max, %)	PDSI (median, %)	Primary land cover
06928000	MO4	MO	3275	1538.7	1.8	12.8	100.0	79.9	DF (45%), HP (43%)
07047950	AR1	AR	1985	1864.2	12.5	20.2	100.0	82.5	CC (73%)
07169500	KS3	KS	2098	1781.3	2.9	4.9	100.0	62.0	H (59%)
07288500	MS1	MS	2009	1809.9	9.8	7.1	97.9	55.9	CCs (82%)
07290000	MS2	MS	7124	2565.5	10.0	13.3	100.0	74.8	EF (19%), MF (19%)
07346070	TX1	TX	1809	2010.3	9.3	6.5	100.0	70.4	HP (27%)
07363500	AR2	AR	5429	1762.5	3.0	28.8	99.1	83.0	EF (40%)
07364200	LA1	AR, LA	3138	1507.9	14.6	22.8	100.0	79.5	CC (31%)
08033500	TX2	TX	9406	1712.0	8.0	3.2	99.9	64.9	EF (29%)
08068090	TX4	TX	2539	1695.0	9.9	10.9	100.0	71.4	EF (32%)
08110000	TX5	TX	2616	1630.0	4.8	8.9	100.0	73.8	HP (55%)
08117500	TX6	TX	1869	1085.4	5.6	6.4	98.6	64.8	HP (43%)
08164000	TX7	TX	2124	1435.4	2.1	8.8	94.1	52.3	HP (59%)
09439000	AZ1	AZ, NM	9279	1679.3	1.2	1.2	98.1	40.2	SS (45%)
09485700	AZ2	AZ	2238	2347.0	2.1	0.0	95.4	48.3	SS (64%)
09487000	AZ3	AZ	2028	3229.6	2.3	0.0	87.7	42.4	SS (79%)
09512800	AZ4	AZ	2876	1639.6	1.3	0.1	88.1	47.1	SS (68%)
09517000	AZ5	AZ	3967	1664.7	1.7	0.2	90.8	50.6	SS (81%)
09537500	AZ6	AZ	2912	1392.5	1.1	0.0	96.6	46.0	SS (67%)
11348500	CA1	CA	3884	1469.4	8.0	0.0	84.1	55.6	SS (50%)
11376000	CA2	CA	2313	2450.2	1.9	0.0	89.1	29.9	SS (56%)
11473900	CA3	CA	1925	4181.6	1.2	0.0	88.2	35.5	EF (45%)
11501000	OR1	OR	4121	1028.4	8.2	0.0	83.3	43.4	EF (55%)
11517500	CA4	CA	2047	1495.8	5.6	0.0	94.6	17.6	EF (37%)
11519500	CA5	CA	1714	2381.7	3.8	0.0	97.6	26.3	EF (46%)
12324680	MT4	MT	4590	1287.2	3.5	1.4	97.7	46.4	EF (45%)
13302005	ID1	ID	2143	1615.5	1.2	0.5	97.8	51.2	SS (76%)
13305000	ID2	ID	2412	1443.0	1.3	0.5	93.6	48.6	SS (59%)
<b>All (median)</b>	~	~	<b>2647</b>	<b>1461.0</b>	<b>5.6</b>	<b>5.0</b>	<b>100.0</b>	<b>62.0</b>	~



775 **Table A2.** Thresholds selected from 5-year Sentinel-1 (S1) and Sentinel-2 (S2) based surface water percentiles to  
 776 account for variable accuracy between sites, sensors, and classes (open water (OW) compared to vegetated water  
 777 (VW)). ~ indicates that this output was excluded from the allowable water mask.

Site ID	S1 OW (%)	S1 VW (%)	S2 OW (%)	S2 VW (%)	Site ID	S1 OW (%)	S1 VW (%)	S2 OW (%)	S2 VW (%)
AR1	15	30	15	30	MN7	10	35	5	25
AR2	5	20	10	25	MN8	10	25	5	15
AZ1	10	5	15	10	MN9	5	25	5	25
AZ2	5	15	10	15	MO1	10	20	10	20
AZ3	5	10	10	15	MO2	5	15	15	25
AZ4	5	20	15	20	MO3	5	30	10	30
AZ5	5	20	20	15	MO4	10	15	10	35
AZ6	10	15	10	~	MS1	10	30	10	35
CA1	5	15	10	20	MS2	5	10	5	30
CA2	10	10	15	15	MT1	25	~	10	30
CA3	10	~	15	15	MT2	25	~	15	40
CA4	10	15	20	20	MT3	30	~	10	40
CA5	10	10	20	15	MT4	30	~	10	30
GA1	5	5	5	20	ND1	15	20	5	10
GA2	5	10	10	15	ND2	20	20	10	20
IA1	~	15	10	15	ND3	15	~	5	20
IA2	~	10	10	20	ND4	15	35	5	30
IA3	10	10	10	20	ND5	20	30	5	25
IA4	10	20	10	20	ND6	15	30	5	25
ID1	30	~	15	35	ND7	20	30	5	20
ID2	30	~	20	35	NE1	15	15	10	20
IL1	10	30	10	15	OR1	10	20	25	25
KS2	10	20	10	30	SC1	5	20	10	35
KS3	~	15	10	20	SC2	5	25	5	25
LA1	10	25	15	35	SC3	5	30	5	30
MD1	5	~	10	20	SC4	5	30	10	35
MD2	5	15	10	20	SD1	10	25	5	25
MD3	5	10	10	15	SD2	15	25	5	25
MD4	5	10	10	15	TX1	5	10	10	30
MD5	10	30	15	~	TX2	5	30	10	35
MN1	15	20	5	20	TX4	5	30	10	35
MN2	10	20	5	30	TX5	5	20	10	~
MN3	10	30	10	30	TX6	10	~	10	35
MN4	5	30	5	30	TX7	5	35	10	30
MN5	10	30	5	25	VA1	5	30	10	45
MN6	15	25	5	20	WI1	~	15	10	20

778



779 **Table A3.** Hydrologic signatures by watershed. The blue to red shading reflects the high to low values for each  
 780 signature. The bold values indicate the average values for the watersheds within each region.

Region	ID	Gage	Flashiness Index	Flashiness index (wet season)	MAX30 /area	(Q10-Q95)/area	Dry Month /area	Baseflow index
<b>East</b>			<b>-0.74</b>	<b>-0.78</b>	<b>1.37</b>	<b>0.023</b>	<b>0.0065</b>	<b>0.38</b>
East	MD1	01491000	-0.48	-0.45	2.16	0.034	0.0072	0.28
	MD2	01578475	-0.44	-0.43	1.52	0.024	0.0105	0.55
	MD3	01580520	-0.52	-0.64	1.45	0.024	0.0112	0.54
	MD4	01594440	-0.43	-0.42	1.38	0.021	0.0089	0.49
	MD5	01643000	-0.35	-0.40	1.98	0.028	0.0058	0.24
	VA1	02049500	-0.87	-1.01	1.27	0.028	0.0060	0.36
	SC1	02131500	-0.66	-0.64	1.29	0.022	0.0059	0.39
	SC2	02135000	-1.05	-1.07	1.55	0.025	0.0055	0.35
	SC3	02136000	-0.91	-1.04	1.22	0.023	0.0039	0.28
	SC4	02175000	-1.13	-1.20	0.89	0.017	0.0055	0.44
	GA1	02198000	-0.90	-0.95	0.86	0.016	0.0043	0.37
	GA2	02202500	-1.09	-1.17	0.92	0.017	0.0030	0.24
<b>Gulf Coast</b>			<b>-0.79</b>	<b>-0.83</b>	<b>1.88</b>	<b>0.032</b>	<b>0.0026</b>	<b>0.09</b>
Gulf Coast	AR1	07047950	-0.99	-1.01	3.48	0.050	0.0057	0.18
	MS1	07288500	-0.79	-0.90	2.23	0.056	0.0035	0.04
	MS2	07290000	-0.85	-0.93	2.22	0.046	0.0030	0.10
	TX1	07346070	-0.74	-0.71	1.64	0.025	0.0006	0.02
	AR2	07363500	-0.82	-0.86	2.46	0.050	0.0024	0.05
	LA1	07364200	-1.45	-1.58	1.37	0.044	0.0030	0.16
	TX2	08033500	-0.94	-1.01	1.19	0.024	0.0027	0.08
	TX4	08068090	-0.35	-0.31	2.30	0.016	0.0022	0.09
	TX5	08110000	-1.00	-1.02	0.54	0.020	0.0024	0.08
	TX6	08117500	-0.51	-0.59	2.10	0.021	0.0019	0.08
	TX7	08164000	-0.21	-0.23	1.13	0.003	0.0010	0.07
<b>Midwest</b>			<b>-0.62</b>	<b>-0.60</b>	<b>1.43</b>	<b>0.021</b>	<b>0.0042</b>	<b>0.28</b>
Midwest	IA1	05388250	-0.78	-0.68	1.51	0.025	0.0083	0.47
	IA2	05412500	-0.73	-0.62	1.53	0.024	0.0066	0.37
	IA3	05418500	-0.80	-0.69	1.11	0.016	0.0077	0.59
	IA4	05422000	-0.99	-1.06	1.14	0.023	0.0060	0.41
	WI1	05434500	-1.12	-1.01	0.96	0.014	0.0094	0.70
	IL1	05447500	-0.79	-0.78	1.03	0.018	0.0055	0.38
	NE1	06815000	-0.25	-0.21	0.96	0.007	0.0013	0.24
	MO1	06821190	-0.52	-0.55	1.14	0.016	0.0018	0.19
	MO2	06908000	-0.40	-0.44	1.61	0.022	0.0010	0.05
	KS2	06916600	-0.55	-0.60	1.48	0.023	0.0013	0.09
	MO3	06918060	-0.39	-0.45	2.13	0.030	0.0020	0.06
	MO4	06928000	-0.38	-0.34	2.24	0.026	0.0024	0.10
	KS3	07169500	-0.42	-0.36	1.69	0.032	0.0015	0.06
<b>North-Central</b>			<b>-0.93</b>	<b>-0.93</b>	<b>0.52</b>	<b>0.008</b>	<b>0.0016</b>	<b>0.19</b>
North-Central	ND1	05056000	-1.04	-0.98	0.11	0.002	0.0005	0.08
	ND2	05057200	-0.83	-0.88	0.21	0.004	0.0004	0.07
	MN1	05062500	-0.94	-0.92	0.48	0.007	0.0014	0.24
	ND3	05066500	-0.76	-0.79	0.54	0.006	0.0007	0.09
	MN2	05078500	-0.81	-0.77	0.54	0.006	0.0011	0.23
	ND4	05090000	-0.78	-0.82	0.34	0.004	0.0004	0.05
	ND5	05123400	-1.09	-1.11	0.10	0.002	0.0001	0.06





Region	ID	Gage	Flashiness		MAX30 /area	(Q10- Q95)/area	Dry Month /area	Baseflow index
			Flashiness Index	index (wet season)				
	MN3	05131500	-0.90	-0.86	1.15	0.018	0.0028	0.19
	MN4	05132000	-1.01	-0.95	0.77	0.013	0.0020	0.27
	MN5	05244000	-1.45	-1.46	0.31	0.006	0.0038	0.68
	MN6	05300000	-0.99	-0.96	0.65	0.011	0.0019	0.21
	MN7	05304500	-1.16	-1.14	0.46	0.010	0.0029	0.34
	MN8	05313500	-0.90	-0.89	0.83	0.015	0.0025	0.18
	MN9	05336700	-0.77	-0.78	1.69	0.027	0.0055	0.25
	ND6	06468170	-0.93	-0.93	0.18	0.003	0.0001	0.04
	ND7	06471200	-0.68	-0.64	0.24	0.002	0.0002	0.09
	SD1	06479525	-1.00	-1.09	0.23	0.005	0.0010	0.22
	SD2	06481500	-0.73	-0.73	0.48	0.009	0.0016	0.18
	<b>Southwest</b>		<b>-0.12</b>	<b>-0.16</b>	<b>0.06</b>	<b>&lt;0.001</b>	<b>&lt;0.0001</b>	<b>0.01</b>
Southwest	AZ1	09439000	-0.61	-0.83	0.09	0.001	0.0000	0.03
	AZ2	09485700	0.07	0.12	0.08	0.000	0.0000	0.00
	AZ3	09487000	0.23	0.23	0.01	0.000	0.0000	0.00
	AZ4	09512800	-0.08	-0.09	0.16	0.001	0.0000	0.00
	AZ5	09517000	-0.30	-0.34	0.02	0.000	0.0001	0.05
	AZ6	09537500	-0.02	-0.03	0.01	0.000	0.0000	0.00
	<b>West</b>		<b>-1.03</b>	<b>-1.09</b>	<b>0.67</b>	<b>0.012</b>	<b>0.0009</b>	<b>0.26</b>
West	MT1	06018500	-1.23	-1.41	0.04	0.001	0.0004	0.44
	MT2	06052500	-1.18	-1.06	0.69	0.013	0.0022	0.32
	MT3	06076690	-1.04	-1.01	0.18	0.004	0.0007	0.32
	CA1	11348500	-0.70	-0.77	0.22	0.004	0.0001	0.02
	CA2	11376000	-0.51	-0.69	1.62	0.023	0.0006	0.06
	CA3	11473900	-0.51	-0.69	3.31	0.051	0.0003	0.01
	OR1	11501000	-1.25	-1.24	0.31	0.005	0.0011	0.35
	CA4	11517500	-1.13	-1.27	0.14	0.003	0.0005	0.21
	CA5	11519500	-0.82	-0.95	0.92	0.023	0.0003	0.03
	MT4	12324680	-1.16	-1.07	0.33	0.006	0.0015	0.38
	ID1	13302005	-1.63	-1.89	0.12	0.002	0.0019	0.61
	ID2	13305000	-1.22	-1.08	0.20	0.003	0.0012	0.40

781

782



783 **Table A4.** Spearman correlation values between remotely sensed surface water variables and other independent  
 784 variables. Significant ( $p < 0.01$ ) correlations, after Bonferroni correction has been applied, are shown shaded in gray.  
 785 CV: coefficient of variation, FP: floodplain, NFP: non-floodplain, temp: temporarily, inun: inundation,  
 786 Geographically Isolated Wetlands: GIW  
 787

Variable Type	Variable	Temp. flooded, FP	Temp. inun., NFP	Seasonally inun., FP	Seasonally inun., NFP	SP-P inun., FP	SP-P inun., NFP	Total inun., FP	Total inun., NFP
Climate	Precipitation (P)	0.39	0.52	0.75	0.44	0.41	0.21	0.69	0.45
	Evapo-transpiration (ET)	0.4	-0.12	0.19	-0.22	-0.1	-0.27	0.19	-0.23
	Aridity index (ET/P)	-0.3	-0.62	-0.66	-0.45	-0.34	-0.14	-0.58	-0.49
	Water demand (P - ET)	0.22	0.61	0.61	0.46	0.34	0.16	0.53	0.5
	Precipitation seasonality	0.03	0.19	0.06	0.29	0.03	0.09	0.11	0.26
	Precipitation CV	-0.02	-0.28	-0.18	-0.03	-0.08	0.06	-0.11	-0.07
	Temperature seasonality	-0.37	0.02	-0.25	0.19	0.06	0.23	-0.21	0.19
	Temperature CV	-0.44	0.02	-0.29	0.17	0.08	0.26	-0.26	0.18
Land cover	Forest	0	0.3	0.1	-0.02	0.06	0	0.04	0.04
	Developed	0.39	0.37	0.63	0.28	0.28	0.04	0.58	0.28
	Cultivated crops	0.07	0.05	0.21	0.28	0.17	0.16	0.23	0.25
	Stream density	0.43	-0.11	0.13	-0.32	-0.24	-0.48	0.13	-0.32
Sub-surface	Clay fraction	0.39	-0.01	0.27	0	0	-0.1	0.27	-0.06
	Sand fraction	-0.35	0.05	-0.17	0.08	0.1	0.22	-0.18	0.09
	Average soil thickness	-0.12	0.33	0.49	0.71	0.66	0.69	0.51	0.68
	Water table depth	-0.18	-0.51	-0.68	-0.78	-0.67	-0.64	-0.72	-0.73
Topography	Slope	0.02	-0.3	-0.55	-0.77	-0.63	-0.76	-0.56	-0.71
	Elevation range	0.21	0.02	0.12	-0.22	-0.13	-0.23	0.04	-0.18
	Topographic diversity	0.02	-0.22	-0.5	-0.71	-0.57	-0.7	-0.51	-0.65
Wetland	GIW	-0.27	0.32	0.37	0.8	0.73	0.89	0.4	0.76
	Proportion of wetland area identified as GIW	-0.09	0.14	0.26	0.55	0.38	0.62	0.29	0.5
	Floodplain	0.64	0.28	0.84	0.36	0.55	0.19	0.92	0.3
	National Wetland Inventory wetlands	-0.27	0.48	0.45	0.81	0.86	0.85	0.46	0.8

788